Table 1
Values used for 3D-CTA segmentation.

Structure	CT value (Hounsfield units)
Lung	<−400
Trachea and bronchus	<−900
Pulmonary vessels	>70
Primary tumor (solid type)	>−100
Primary tumor (non-solid type)	>−700

CT, computed tomography; 3D-CTA, three-dimensional computed tomography angiography.

bronchi and vessels. Finally, the virtual safety margin was merged with the 3D-CTA image. The safety margin was defined as a sphere, extending 2 cm outside the primary tumor; for example, the margin was 6 cm in diameter for a primary tumor of 2 cm. The center of the virtual safety margin was manually matched to the center of the tumor using the 3D workstation. The chest radiologist interpreted the relationship between the margin and the intersegmental veins and used this to recommend the minimal extent of segmentectomy for each patient. In cases where the intersegmental veins ran through the safety margin, the veins were designated for removal. It took about 1.5 h to construct 3D-CTA with a virtual safety margin and to report the recommendation per patient. The 3D images and the radiologist's report were delivered to the intra-institutional picture archiving and communication system; the surgeons had this information available at the preoperative conference and in the operating room. Each patient's procedure was planned based on the radiological report and the 3D-CTA image with a virtual safety margin; the actual operating procedure was adjusted, if necessary, based on the surgical findings. After thoracotomy, the surgeons touched the primary tumor directly and confirmed eventually the enough resection margin ≥2 cm. In addition, the actual surgical margins that were the shortest distance between the tumor and the surgical cut surface were measured on the formalin-fixed specimen.

2.4. Assessment of 3D-CTA with a virtual safety margin

We compared the planned procedure with the actual segmentectomy procedure performed in each patient. We also evaluated the postoperative pathologic findings, with particular attention to whether there was residual tumor on the specimen's surgical margin. The tumor size on preoperative CT was compared with the actual size of the pathological specimen using Pearson's correlation coefficient.

3. Results

Of 226 thoracic surgeries for primary lung cancer conducted at our institution in the study timeframe, a total of 17 tumors in 16 patients qualified for this study, as they were removed by segmentectomy planned with preoperative 3D-CTA with a virtual safety margin (Table 2). The patients comprised 11 males and 5 females, aged 52 to 82 years. One patient had 2 simultaneous cancers in the left upper and lower lobe and underwent each segmentectomy on a same operation (Cases 5 and 11). The tumor size on preoperative thin-section CT ranged from 1.0 to 2.0 cm in maximal diameter, while that of the surgical specimens ranged from 0.7 to 2.3 cm. There was a strong correlation between the CT image size and that of the surgical specimens ($r = 0.75$; $p < 0.001$). Sixteen tumors located in peripheral area within 2.5-cm of the chest wall and one tumor (Case 6) located in the intermediate area. The internal opacity was non-solid in 6 tumors, partly solid in 3 tumors, and solid in 8 tumors. The reason to plan the segmentectomy for solid type tumors were previous or simultaneous lung cancer in 5 patients (Case 10, 11, 12, 15, 17), complication of COPD in one patient (Case 16), and advanced age in one patient (Case 13). Remaining one patient (Case 14) chose for segmentectomy instead of lobectomy after fully discussing the risk and benefits with the surgeons.

In 10 of 17 tumors (59%) segmentectomy was performed without deviation from the preoperative plan. In 5 tumors (29%), segmentectomy was performed with a wider margin than the preoperative plan called for. In 4 of these 5 cases (Cases 6, 7, 9, 11), left S1+2 segmentectomy was planned but left upper division segmentectomy was actually performed; the upper division segmentectomy was chosen in these cases as it was surgically more facile due to a single intersegmental dissection surface than S1+2 segmentectomy [4]. In Case 4, left S3+S4 segmentectomy was planned but left S3+S4+S5 was performed due to the small volume of residual S5 and the risk of torsion. In 2 cases (12%), a more limited segmentectomy was performed (Cases 3 and 14) because the radiologist did not take subsegmental resection into consideration when making surgical recommendations.

The actual surgical margins ranged from 1.5 to 5.0 cm (median 3.3 cm) on formalin-fixed specimen. Pathological examination revealed no residual tumor cells at the surgical margins and no lymph node metastases in any patients. The pathological stages were T1aN0M0 ($n = 14$), T2a(pl1)N0M0 ($n = 2$), and T3a(pl3)N0M0 ($n = 1$). One patient was hospitalized for 20 days after surgery because of drug-induced liver dysfunction; no other patients experienced complications.

Table 2
Patient characteristics.

Case	Sex	Age	Internal opacity	Size (cm)	Side	Planned procedure	Actual procedure	Pathology	Actual margin (cm)
1	F	68	NS	1.4	Right	S1	S1	W/D AC	3.0
2	M	70	NS	1.5	Left	S1+2	S1+2	W/D AC	1.5
3	F	71	NS	1.7	Right	S1+S2	S1+S2a	W/D AC	3.0
4	F	73	NS	1.8	Left	S3+S4	S3+S4+S5	M/D AC	2.0
5	M	68	NS	1.9	Left	S6	S6	W/D AC	2.0
6	M	70	NS	2.0	Left	S1+2	S1+2+S3	W/D AC	4.0
7	M	70	PS	1.2	Left	S1+2	S1+2+S3	W/D AC	5.0
8	F	53	PS	1.5	Right	S1+S2	S1+S2	W/D AC	1.5
9	M	63	PS	2.0	Left	S1+2	S1+2+S3	M/D AC	Not available
10	M	70	SOL	1.0	Right	S6	S6	M/D AC	2.5
11	M	68	SOL	1.0	Left	S1+2	S1+2+S3	M/D AC	3.5
12	M	52	SOL	1.1	Left	S1+2+S3	S1+2+S3	M/D AC	4.0
13	F	82	SOL	1.2	Left	S1+2+S3	S1+2+S3	M/D AC	4.5
14	M	60	SOL	1.3	Right	S6+S10	S6+S10a	M/D AC	2.0
15	M	67	SOL	1.5	Right	S6	S6	M/D SCC	3.5
16	M	56	SOL	1.6	Left	S1+2+S3	S1+2+S3	M/D SCC	5.0
17	M	62	SOL	1.8	Left	S1+2	S1+2	M/D AC	3.5

M/D AC, moderately differentiated adenocarcinoma; M/D SCC, moderately differentiated squamous cell carcinoma; NS, non-solid; PS, partly solid; SOL, solid; W/D AC, well-differentiated adenocarcinoma; S2a, posterior subsegment of S2; S10a, posterior subsegment of S10.

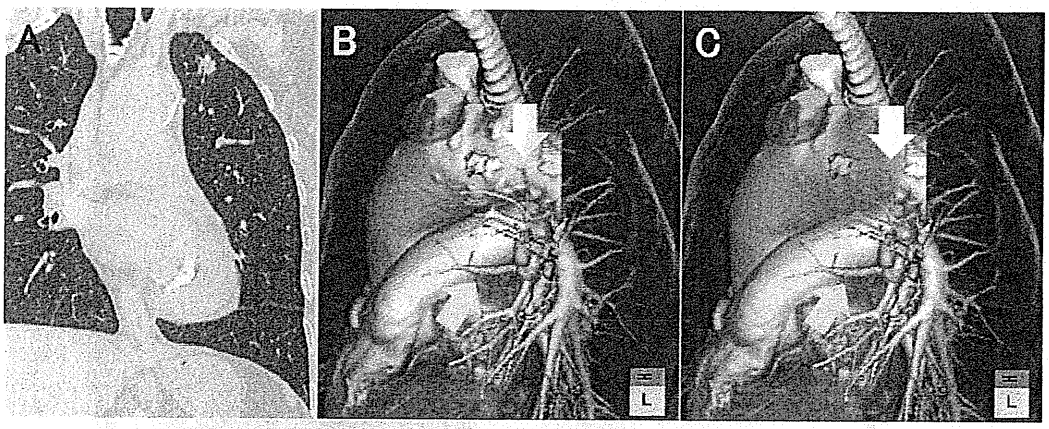

Fig. 2. An 82-year-old female. (A) A solid lung cancer in the left S1+2 segments is seen on coronal CT; the maximal tumor diameter is 1.2 cm. (B) 3D-CTA of the left upper lobe. The relevant intersegmental veins are V3b, between S3 and S4 (yellow arrow), and V1b, between S1+2 and S3 (white arrow). (C) 3D-CTA with the virtual safety margin. Because V3b is running through the margin but V1b is running within it, S1+2+S3 segmentectomy is necessary. (For interpretation of the references to color in this figure legend, the reader is referred to the web version of the article.)

Fig. 2 displays images for Case 13, an 82-year-old female. She had a solid lung cancer in the left S1+2 segments; the maximal tumor diameter was 1.2 cm. Based on 3D-CTA with a virtual safety margin and given her advanced age, we planned and performed segmentectomy of the left upper division. The pathologic findings confirmed the diagnosis of moderately differentiated adenocarcinoma, pT1aN0M0; the surgical margins were negative for tumor cells. She had no postoperative complications.

Fig. 3 displays the images for Case 1, a 68-year-old female. She had a non-solid lung cancer located in the right S1 segment with a maximal tumor diameter of 1.4 cm. Based on 3D-CTA with a virtual safety margin, we planned and performed right S1 segmentectomy. The pathologic findings confirmed the diagnosis of well-differentiated adenocarcinoma, pT1aN0M0; the surgical margins were negative. She had no postoperative complications.

Fig. 4 displays the images for Case 9, a 63-year-old male. He had a partly solid lung cancer located in the left S1+2 segments; the maximal tumor diameter was 2.0 cm. The radiologist suggested left S1+2 segmentectomy because the intersegmental vein between S1+2 and S3 appeared distant enough from the virtual safety margin. The surgeon eventually selected segmentectomy of the left upper division (S1+2+S3). The pathologic findings confirmed the diagnosis of moderately differentiated adenocarcinoma, pT2a(pl1)N0M0; the surgical margins were negative. He had no postoperative complications.

4. Discussion

3D-CTA with a virtual safety margin is a non-invasive method of visualizing not only the branching of bronchi and pulmonary arteries and veins, but also the three-dimensional distances and relationships between the primary tumor and the intersegmental pulmonary veins. This technology could therefore be useful in preoperative planning of a suitable segmentectomy procedure in lung cancer patients. We found that thoracic surgeons were usually able to perform segmentectomy according to the preoperative plan. In the present study, no positive surgical margins were observed.

Segmentectomy could increase the risk of locoregional recurrence at the resection line, compared with lobectomy [3,11–13]; inadequate safety surgical margins and incomplete lymph node clearance are identified as the main causes for this recurrence. Because there are intersegmental veins but no pleura between segments, a sufficient surgical margin must be secured by segmentectomy. As the lung parenchyma is dissected along the intersegmental vein, this vein should not pass through the safety margin; however, during surgery on a contracted lung it can be

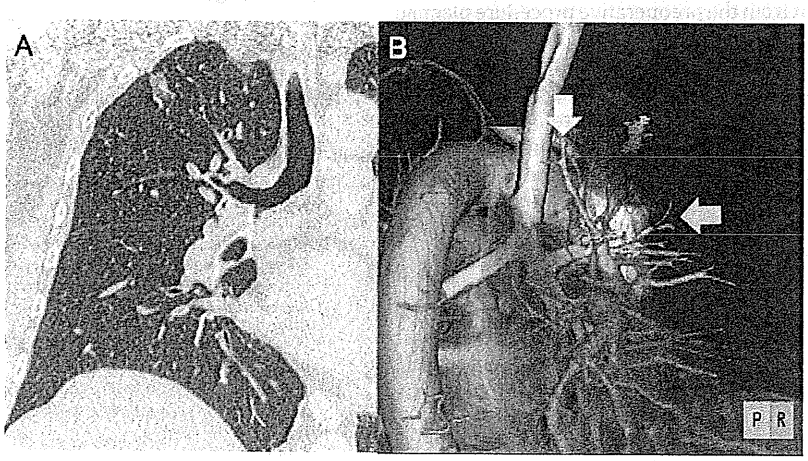

Fig. 3. A 68-year-old female. (A) A non-solid lung cancer in the right S1 segment is seen on coronal CT; the maximal tumor diameter is 1.4 cm. (B) 3D-CTA with the virtual safety margin. The relevant intersegmental veins are V1b, between S1 and S3 (yellow arrow), and V2a, between S1 and S2 (white arrow). Because both intersegmental veins are running outside of the virtual safety margin, S1 segmentectomy is able to be performed. (For interpretation of the references to color in this figure legend, the reader is referred to the web version of the article.)

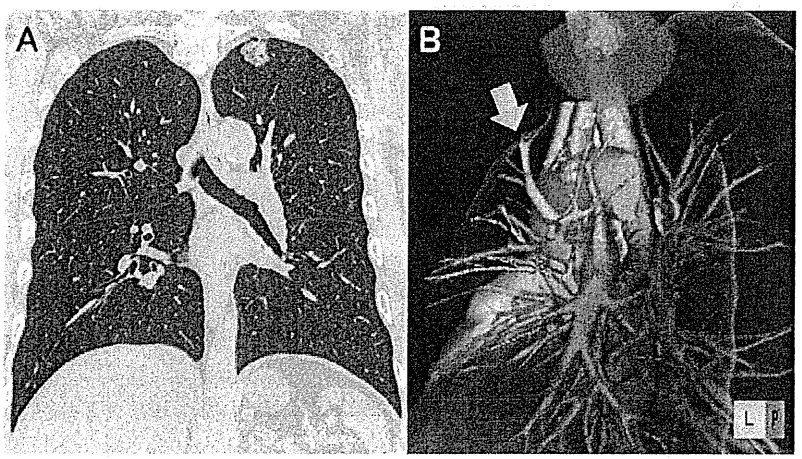

Fig. 4. A 63-year-old male. (A) A partly solid lung cancer in the left S1 + 2 segments is seen on coronal CT; the maximal tumor diameter is 2.0 cm. (B) 3D-CTA with the virtual safety margin. The relevant intersegmental vein is V3b, between S1 + 2 and S3 (yellow arrow). Because the intersegmental vein is running outside of the virtual safety margin, S1 + 2 segmentectomy is able to be performed. (For interpretation of the references to color in this figure legend, the reader is referred to the web version of the article.)

difficult for surgeons to recognize the relationship between the safety margin and the intersegmental veins. Preoperative planning to decide on a minimal resection extent is therefore important in segmentectomy.

We adopted a distance of 2 cm from the tumor surface as our virtual surgical margin [10]. Safety margins of 2 cm or larger are usually adequate to prevent local recurrence when the tumor is smaller than 2 cm [8,9]. In our study, 14 tumors could keep the actual surgical margins of at least 2 cm. Although the margins of 2 tumors were 1.5 cm, the reason may be that the distance was measured on the deflated and fixed specimens. Furthermore, no residual tumor cells were seen at the surgical margins for any type of tumor, whether solid, non-solid, or partly solid. Small tumors with a diameter of ≤2 cm and non-solid tumors are radiologically determined to be non-invasive cancer [1,8]. Partly solid and solid tumors are supposed to have invasive potential, even if they are small in size; adequate surgical safety margins for these invasive small tumors are controversial. Based on our limited results, a virtual surgical margin of 2 cm from the tumor surface may be adequate for not only non-solid tumors, but also partly solid and solid lung cancers that measure ≤2 cm in maximum diameter on thin-section CT. Further case evaluations are needed to verify this observation.

Seven patients in this study underwent an actual segmentectomy procedure different from the preoperative procedure planned using the virtual 3D safety margin. In 4 cases, the left S1 + 2 segmentectomy suggested by the radiologist was modified to a left upper division segmentectomy. Because the left upper division segmentectomy is typical procedure of segmetectomy, it has been performed more than S1 + 2 segmentectomy in our institution even if the safety margin is sufficient (Fig. 4). Although the virtual safety margin indicates the minimal extent of resection, the actual procedure should be determined by the surgeon in real time, as many other factors can affect the surgery.

Obtaining a virtual safety margin is simple and non-invasive; the primary tumor and the spherical safety margin are superimposed on a 3D-CTA image. At most of the hospital, the contrast enhanced CT is scanned routinely to evaluate hilar and mediastinal lymph node enlargement in lung cancer patients. We think that most 3D workstations are able to create this margin because it requires only basic workstation functions. In the present study, a chest radiologist constructed the 3D-CTA and manually merged it with a virtual safety margin. This was time-consuming work, but in the near future computers may be able to automatically construct a virtual safety margin when 3D-CTA is performed.

This retrospective study is limited by being an initial report; we were not able to examine the long-term outcomes or prognoses of these segmentectomy patients. Long-term follow up is essential to determine whether 2 cm is an adequate virtual surgical margin [14]. It is also necessary to investigate the usefulness of this method in patients with tumors >2 cm in diameter.

In conclusion, 3D-CTA with a virtual safety margin is able to non-invasively visualize three-dimensional distances and relationships between primary tumors and intersegmental pulmonary veins. It aids in the preoperative planning of suitable segmentectomy procedures for patients with primary lung cancer, when the tumor is 2 cm or less in diameter.

Funding

This work was supported by a Grant-in-Aid for Scientific Research on Innovative Areas from the Japanese Ministry of Education, Culture, Sports, Science and Technology (MEXT).

Conflict of interest

None of the authors have any conflicts of interest associated with this study.

References

[1] Nakamura K, Saji H, Nakajima R, Okada M, Asamura H, Shibata T, et al. A phase III randomized trial of lobectomy versus limited resection for small-sized peripheral non-small cell lung cancer (JCOG0802/WJOG4607L). Jpn J Clin Oncol 2010;40:271–4.
[2] Keenan RJ, Landreneau RJ, Maley Jr RH, Singh D, Macherey R, Bartley S, et al. Segmental resection spares pulmonary function in patients with stage I lung cancer. Ann Thorac Surg 2004;78:228–33.
[3] Nomori H, Mori T, Ikeda K, Yoshimoto K, Iyama K, Suzuki M. Segmentectomy for selected cT1N0M0 non-small cell lung cancer: a prospective study at a single institute. J Thorac Cardiovasc Surg 2012;144:87–93.
[4] Oizumi H, Kanauchi N, Kato H, Endoh M, Suzuki J, Fukaya K, et al. Anatomic thoracoscopic pulmonary segmentectomy under 3-dimensional multidetector computed tomography simulation: a report of 52 consecutive cases. J Thorac Cardiovasc Surg 2011;141:678–82.
[5] Oizumi H, Endoh M, Takeda S, Suzuki J, Fukaya K, Sadahiro M. Anatomical lung segmentectomy simulated by computed tomographic angiography. Ann Thorac Surg 2010;90:1382–3.
[6] Shimizu K, Nakano T, Kamiyoshihara M, Takeyoshi I. Segmentectomy guided by three-dimensional computed tomography angiography and bronchography. Interact Cardiovasc Thorac Surg 2012;15:194–6.
[7] Yamashita H. Variations in the pulmonary segments and the bronchovascular trees. In: Yamashita H, editor. Roentgenologic anatomy of the lung. Tokyo: Igaku-shoin; 1978. p. 70–107.

[8] Suzuki K, Koike T, Asakawa T, Kusumoto M, Asamura H, Nagai K, et al. A prospective radiological study of thin-section computed tomography to predict pathological noninvasiveness in peripheral clinical IA lung cancer (Japan Clinical Oncology Group 0201). J Thorac Oncol 2011;6:751–6.
[9] Swanson SJ. Segmentectomy for lung cancer. Semin Thorac Cardiovasc Surg 2010;22:244–9.
[10] Iwano S, Usami N, Yokoi K, Naganawa S. Segmentectomy simulation using a virtual three-dimensional safety margin. Ann Thorac Surg 2012;93:e37–9.
[11] El Sherif A, Gooding WE, Santos R, Pettiford B, Ferson PF, Fernando HC, et al. Outcomes of sublobar resection versus lobectomy for stage I non-small cell lung cancer: a 13-year analysis. Ann Thorac Surg 2006;82:408–15.
[12] Sienel W, Stremmel C, Kirschbaum A, Hinterberger L, Stoelben E, Hasse J, et al. Frequency of local recurrence following segmentectomy of stage IA non-small cell lung cancer is influenced by segment localisation and width of resection margins—implications for patient selection for segmentectomy. Eur J Cardiothorac Surg 2007;31:522–7.
[13] Miller DL, Rowland CM, Deschamps C, Allen MS, Trastek VF, Pairolero PC. Surgical treatment of non-small cell lung cancer 1 cm or less in diameter. Ann Thorac Surg 2002;73:1545–50.
[14] Nakao M, Yoshida J, Goto K, Ishii G, Kawase A, Aokage K, et al. Long-term outcomes of 50 cases of limited-resection trial for pulmonary ground-glass opacity nodules. J Thorac Oncol 2012;7:1563–6.

Role of lymphatic invasion in the prognosis of patients with clinical node-negative and pathologic node-positive lung adenocarcinoma

Takahiro Mimae, MD, PhD,[a] Yasuhiro Tsutani, MD, PhD,[a] Yoshihiro Miyata, MD, PhD,[a] Tomoharu Yoshiya, MD,[a] Yuta Ibuki, MD,[a] Kei Kushitani, MD, PhD,[b] Yukio Takeshima, MD, PhD,[b] Haruhiko Nakayama, MD, PhD,[c] Sakae Okumura, MD, PhD,[d] Masahiro Yoshimura, MD, PhD,[e] and Morihito Okada, MD, PhD[a]

Objective: Some patients with clinical T1 N0 M0 lung adenocarcinoma have pathologic lymph node metastasis. However, neither the precise prognosis nor the factors predictive of the prognosis of such patients have yet been identified.

Methods: Our study included 609 patients with clinical T1 N0 M0 lung adenocarcinoma; 568 (93.3%) pathologic node negative [pN(–)] and 41 (6.7%) pathologic node positive [pN(+)] patients, diagnosed after complete surgical resection. The association between prognosis and pathologic findings was analyzed retrospectively.

Results: pN(+) patients had a significantly lower lepidic growth component ratio (10% vs 50%), a higher lymphatic invasion (LI) rate (68% vs 11%), vessel invasion rate (59% vs 14%), and visceral pleural invasion rate (29% vs 9%), compared with pN(–) patients (all *P*s < .001). Surprisingly, 13 of 41 (32%) pN(+) patients showed no LI. In pN(–) patients, a multivariate analysis of recurrence-free survival revealed that lower lepidic growth component ratio, and lymphatic, vessel, and pleural invasion were significantly correlated with a poor prognosis ($P = .008$, .045, .031, and .024). However, in pN(+) patients, the multivariate analysis of recurrence-free survival showed that only LI was a significant independent prognostic factor ($P = .037$). The 5-year recurrence-free survival rates were as follows: 91.2% for pN(–)/LI(–) patients, 68.2% for pN(–)/LI(+) patients, 63.5% for pN(+)/LI(–) patients, and 41.9% for pN(+)/LI(+) patients. LI status stratified the prognosis not only in patients with no nodal metastasis but also in those with metastasis.

Conclusions: LI, which is not always present in node-positive adenocarcinoma, is an important prognostic variable in patients with node involvement. (J Thorac Cardiovasc Surg 2014;147:1820-6)

Fluorescence deoxyglucose (FDG) positron emission tomography (PET) is commonly used for preoperative assessment of primary tumors, lymph nodes, and distant metastasis to determine staging and treatment strategy,[1-3] thereby improving the accuracy of the definition of clinical stage IA compared with only computed tomography assessment.[1] This has changed the population of patients with clinical stage IA lung adenocarcinoma.[1,4-7] However, some clinical lymph node-negative [cN(–)] patients show positive pathologic lymph node [pN(+)] metastasis. It is speculated that a cN(–) but pN(+) status indicates an initial lymph node metastatic condition, because the accumulation of FDG in the lymph node could be significantly higher in patients with massive lymph node metastasis. Therefore, cN(–)/pN(+) patients may have a better prognosis than cN(+)/pN(+) patients, or a similar prognosis to cN(–)/pN(–) patients. In addition, no studies have identified the prognostic factors in cN(–)/pN(+) patients.

In our study, we evaluated the clinicopathologic findings and prognosis of patients with clinical T1 N0 M0 lung adenocarcinoma according to lymph node status, or other pathologic status. First, we examined the pathologic findings to identify predictive factors for recurrence-free survival (RFS) among patients with clinical stage IA lung adenocarcinoma. Multivariate analysis revealed that lymphatic invasion (LI) status was a predictive factor, both in patients with and without node involvement. Next, we assessed the prognosis of patients with and without lymph node involvement according to LI status. The results highlight the importance of the LI status in patients with clinical T1 N0 M0 lung adenocarcinoma.

MATERIALS AND METHODS

Patient Population

Our study included 611 patients who underwent complete surgical resection of clinical stage IA lung adenocarcinoma at the Hiroshima University

From the Departments of Surgical Oncology[a] and Pathology,[b] Hiroshima University, Hiroshima, Japan; Department of Thoracic Surgery,[c] Kanagawa Cancer Center, Yokohama, Japan; Department of Thoracic Surgery,[d] Cancer Institute Hospital, Tokyo, Japan; and Department of Thoracic Surgery,[e] Hyogo Cancer Center, Akashi, Japan.

Disclosures: Authors have nothing to disclose with regard to commercial support.
Received for publication Aug 5, 2013; revisions received Oct 22, 2013; accepted for publication Nov 22, 2013; available ahead of print Feb 7, 2014.

Address for reprints: Morihito Okada, MD, PhD, Department of Surgical Oncology, Hiroshima University, Hiroshima, Japan, 1-2-3 Kasumi, Minami-ku, Hiroshima, 734-8551, Japan (E-mail: morihito1217@hiroshima-u.ac.jp).

0022-5223/$36.00

http://dx.doi.org/10.1016/j.jtcvs.2013.11.050

Abbreviations and Acronyms

CT = computed tomography
FDG = fluorescence deoxyglucose
GGO = ground glass opacity
HU = Haunsfield unit
LC = lepidic component
LI = lymphatic invasion
OS = overall survival
PET = positron emission tomography
RFS = recurrence-free survival
SUV = standardized uptake value

Hospital (Hiroshima, Japan), the Kanagawa Cancer Centre (Yokohama, Japan), the Cancer Institute Hospital (Tokyo, Japan), and the Hyogo Cancer Centre (Akashi, Japan) between April 2007 and December 2010. Approval was given by the institutional review boards of the participating institutions, all of which waived the requirement for informed consent from individual patients for this retrospective review of the prospective database. Two patients were excluded because they lacked a lepidic component (LC) ratio. The data from the remaining 609 patients were analyzed retrospectively. High-resolution computed tomography (CT) and FDG-PET/CT, followed by a curative R0 resection were performed for all patients staged according to the TNM Classification of Malignant Tumours.[8] Endobronchial ultrasonography or mediastinoscopy was not performed routinely because all patients underwent preoperative high-resolution CT and FDG-PET/CT; the high-resolution CT results showed no swelling of mediastinal or hilar lymph nodes and FDG-PET revealed no accumulation of FDG in those lymph nodes. Lymph node swelling was defined when the diameter of a minor axis is larger than 10 mm. Sublobar resection was performed in cases of complete removal of the disease with appropriate surgical margins for a peripheral T1a N0 M0 tumor. Wedge resection without lymph node assessment was performed for ground glass opacity (GGO) tumors on high-resolution CT, which was regarded as a node-negative and noninvasive tumor in a prospective study.[9] Segmentectomy with hilar and mediastinal lymph node dissection were performed for a GGO-mixed tumor. If lymph node involvement was detected on an intraoperative frozen section of any lymph node, the procedure was converted to a standard lobectomy. All other patients underwent a standard lobectomy. The inclusion criteria included preoperative staging determined by high-resolution CT and FDG-PET/CT, curative surgery without any induction therapy, and a definitive histopathologic diagnosis of lung adenocarcinoma. Patients with incompletely resected tumors (R1 or R2), and those with multiple tumors or previous lung surgery, were excluded from the data set.

Pathology Studies

Sections were fixed with 10% formalin and embedded in paraffin. Consecutive 4-μm sections were cut and 1 slice per 5 mm was examined under a microscope for the pathologic assessment. Histologic diagnosis and staging was based on the latest edition of the World Health Organization classification scheme.[10] The histologic type of adenocarcinoma and the presence of lymphatic involvement were determined using hematoxylin-eosin stained tissue. If the findings could not be determined by hematoxylin-eosin staining alone, immunohistochemical staining was carried out as necessary. An LC ratio was defined as the proportion of LC area relative to the entire tumor. LI and blood vessel invasion were assessed by immunohistochemistry for D2-40, which stains lymphatic ducts, and Van Gieson staining of the elastic fiber of the vessels. LI and blood vessel invasion were determined when spreading through or penetration was detected as an extension of a malignant neoplasm. To evaluate pleural invasion, elastic tissue fibers were subjected to Van Gieson staining. Pleural invasion was determined if cancer cells had invaded beyond the elastic layer, including invasion into the visceral pleural surface, or neighboring organs. Histologic examinations were determined by pathologists from each institution for the purposes of this study.

HRCT

A 16-row multidetector CT was used to obtain chest images. For high-resolution images of the tumors, the following parameters were used: 120 kVp, 200 mA, 1 to 2 mm section thickness, 512 × 512 pixel resolution, 0.5 to 1.0 second scanning time, a high spatial reconstruction algorithm with a 20 cm field of view, and mediastinal (level, 40 Haunsfield unit [HU]; width, 400 HU) and lung (level, −600 HU; width, 1600 HU) window settings. GGO was defined as a misty increase in lung attenuation that did not obscure underlying vascular markings. CT scans were reviewed and tumor sizes determined by radiologists from each institution.

FDG-PET/CT

Patients were instructed to fast for at least 4 hours before intravenous injection of 74 to 370 MBq FDG and then to relax for at least 1 hour before the FDG-PET/CT scan. For imaging, Biograph Sensation 16 (Siemens Healthcare, Erlangen, Germany), Aquiduo (Toshiba Medical Systems Corporation, Tochigi, Japan), or Discovery ST (GE Healthcare, Little Chalfont, United Kingdom) integrated 3-dimensional PET/CT scanners were used. Low-dose nonenhanced CT images of 2 to 4 mm section thickness were taken from the head to the pelvis of each patient. An anthropomorphic body phantom (NEMA NU2-2001; Data Spectrum Corp, Hillsborough, NC) was used to minimize variations in standardized uptake values (SUVs) among the institutions.[11,12] The original SUV_{max} values were determined by radiologists from each institution for the purposes of this study. On FDG-PET/CT images, all lymph nodes in the thorax with FDG uptake no greater than the normal background activity of the mediastinal blood pool—the SUV_{max} of which was <1.5, regardless of size—were considered cN0. A lymph node where the SUV_{max} was ≥1.5 or more was considered "suspicious for malignancy." However, even lymph nodes with high FDG uptake, when they showed higher attenuation than mediastinal structures (great vessels) or benign calcification (central, nodular, diffuse, or popcorn-like), were also considered benign.[13]

Follow-up Evaluation

All patients who underwent lung resections were followed-up from the day after surgery. Postoperative follow-up procedures, including a physical examination and chest radiograph every 3 months and chest and abdominal CT examinations every 6 months, were performed for the first 2 years. Thereafter, a physical examination and chest radiograph were performed every 6 months, and a chest CT examination was performed annually.

Statistical Analyses

Patients with clinical stage IA lung adenocarcinoma were included in the analysis. A Mann-Whitney *U* test was used to compare continuous variables and the χ^2 test or Fisher exact test was used for categorical variables. RFS was defined as the length of time after primary surgical treatment for a cancer ends that the patient survived without any sign or symptom of the cancer. Recurrence was defined as patients having symptoms caused by recurring cancer and suspicious lesions that were diagnosed as recurrent tumors by biopsies. If suspicious lesions were not diagnosed as recurrence, by biopsy, the "recurrence" was comprehensively and clinically defined by radiographic findings, including CT and FDG-PET/CT. RFS and overall survival (OS) curves were calculated using the Kaplan-Meier method. Univariate survival analysis was performed using the log-rank test for comparisons of curves. A Cox regression model was used to calculate *P* values and hazard ratios in the univariate and multivariate analyses. The prognostic analysis was performed during August 2012. All statistical analyses were

GTS

performed using EZR (Saitama Medical Centre, Jichi Medical University, Saitama, Japan),[14] which is a graphical user interface for R (The R Foundation for Statistical Computing, version 2.13.0, Vienna, Austria). More precisely, it is a modified version of R Commander (version 1.6-3), which includes statistical functions frequently used in biostatistics.

RESULTS

Clinical Outcomes in Patients With Lung Adenocarcinoma

The median follow-up time was 41.6 months. Lobectomy, segmentectomy, and wedge resection were performed in 375, 97, and 137 patients, respectively. The 30-day mortality rate was 0%. As shown in Table 1, 41 patients (6.7%) had lymph node metastasis in the clinical stage IA lung adenocarcinoma cohort. No significant difference between pN(–) and pN(+) patients was detected in terms of age, sex, and carcinoembryonic antigen value, whereas a marginal difference was seen for tumor size on preoperative high-resolution CT. Regarding the clinical variables, lower GGO ratios and higher SUV_{max} were observed in the N+ group compared with the N– group. In terms of pathologic variables, a lower LC ratio and higher positive rate of LI, blood vessel invasion, and pleural invasion were detected in pN(+) patients. Thirteen of 41 pN(+) patients showed no LI. As shown in Figure 1, *A*, clinical stage IA lung adenocarcinoma patients with lymph node metastasis had a lower RFS rate than those without lymph node metastasis ($P < .001$).

Univariate and Multivariate Analyses of Prognosis According to Pathologic Variables, by Lymph Node Status

Univariate and multivariate analyses of the clinical and pathologic variables were performed to ascertain the most important predictive factor. Univariate analyses were performed on RFS and OS, whereas further analyses, including multivariate analyses, were performed on RFS because OS was more immature than RFS. The pathologic variables included LC ratio, LI status, blood vessel invasion status, pleural invasion status, and lymph node status. For the LC ratio, 30% was used as a threshold because this is the borderline for cT1 N0 M0 lung adenocarcinoma classified as a high- or low-grade malignancy.[2] Univariate analysis revealed that pN(+) patients with LI positive status [LI(+)] had a marginally poorer prognosis ($P = .059$), whereas a lower LC ratio and LI+ status, blood vessel invasion, pleural invasion, or lymph node metastasis was significantly correlated with a poor prognosis in both all patients in this cohort, and in pN(–) patients (Table 2). Additionally, multivariate analysis showed that only LI positive status was a prognostic factor in pN(+) patients ($P = .037$), whereas a lower LC ratio and positive LI status, blood vessel invasion, pleural invasion, or lymph node metastasis were prognostic factors in both all patients and pN(–) patients (Table 3).

TABLE 1. Clinicopathologic findings in patients with clinical stage IA lung adenocarcinoma with or without lymph node metastasis

Finding	Node negative (n = 568)	Node positive (n = 41)	*P* value
Age			
Median	66	65	.33
Interquartile range	60.75-73	56-73	
Sex			
Female	322 (57%)	22 (54%)	.19
Male	246 (43%)	19 (46%)	
CEA			
Median	2.5	3.6	.25
Interquartile range	1.5-3.6	1.1-113.8	
Size*			
Median	2.0	2.2	.060
Interquartile range	1.5-2.4	2.55-4.2	
GGO† ratio			
Median	40	0	<.001
Interquartile range	10-80	0-10	
SUV max			
Median	1.5	3.6	<.001
Interquartile range	0.9-2.6	2.3-4.9	
LC ratio			
Median	50	10	<.001
Interquartile range	10-90	0-20	
Lymphatic invasion			
Negative	507 (89%)	13 (32%)	<.001
Positive	61 (11%)	28 (68%)	
Blood vessel invasion			
Negative	488 (86%)	17 (41%)	<.001
Positive	80 (14%)	24 (59%)	
Pleural invasion			
Negative	515 (91%)	29 (71%)	<.001
Positive	53 (9%)	12 (29%)	

CEA, Carcinoembryonic antigen; *GGO*, ground-glass opacity; *SUV*, standardized uptake value; *LC*, lepidic component. *Tumor size on the high-resolution computed tomography scan. †GGO ratio on the high-resolution computed tomography scan.

Next, we assessed the RFS of pN(–) and pN(+) patients according to their LI status. In both pN(–) and pN(+) patients, RFS rates were lower in LI(+) status compared with LI negative status [LI(–)] ($P < .001$ and $P = .059$) (Figure 1, *B* and *C*). The 3-year RFS and OS rates for each group was as follows: pN(–)/LI(–) 93.4% and 96.7%, pN(–)/LI(+) 70.8% and 85.1%, pN(+)/LI(–) 84.6% and 92.3%, and pN(+)/LI(+) 47.9% and 75.0%, respectively (Table 2 and Figure 1, *B-F*). No significant difference was detected between the pN(+)/LI(–) and pN(–)/LI(+) patients for RFS ($P = .62$; Figure 1, *D*), whereas pN(+)/LI(–) and pN(–)/LI(–) patients, pN(+)/LI(+) and pN(–)/LI(–) patients, and pN(+)/LI(+) and pN(–)/LI(+) patients exhibited significantly different RFS values ($P = .022$, <.001, and .011, respectively).

Clinicopathologic Findings in N+ Patients

In N+ patients, there were no significant differences between the LI(–) and LI(+) groups in terms of age, sex,

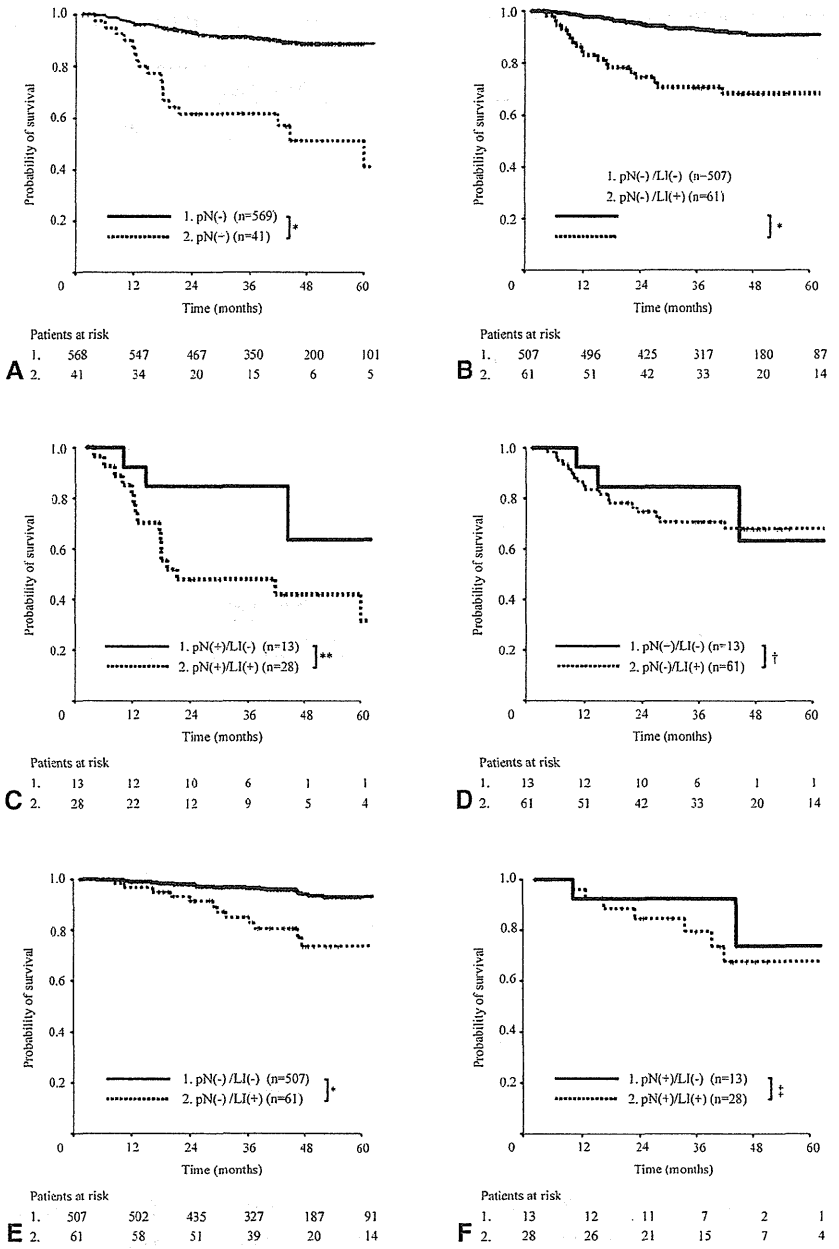

FIGURE 1. Kaplan-Meier recurrence-free survival (A-D) and overall survival (E and F) curves in patients with clinical stage IA lung adenocarcinoma according to pathologic lymph node status and lymph node metastasis and lymphatic invasion (*LI*) status. A, Patients are classified into pathologic lymph node metastasis negative (pN[−]) and positive (pN[+]) groups. B, The pN(−) patients are classified into a lymphatic permeation negative (pN[−]/LI[−]) group and a lymphatic permeation positive (pN[−]LI[+]) group. C, The pN(+) patients are classified into a lymphatic permeation negative (N[+]LI[−]) group and a lymphatic permeation positive (N[+]LI[+]) group. D, Recurrence-free survival curves of pN(+)LI(−) and pN(−)LI(+) patients are shown. E, The pN(−) patients are classified into a pN(−)/LI(−) group and a pN(−)LI(+) group. F, The pN(+) patients are classified into an N(+)LI(−) group and an N(+)LI(+) group. *$P < .001$; **$P = .059$; †$P = .62$; ‡$P = .48$.

carcinoembryonic antigen values, preoperative tumor size, and SUV_{max} values. Regarding pathologic findings, LI status had no association with the LC ratio, blood vessel invasion, and pleural invasion. Additionally, LI status had no correlation with lymph node metastasis status, both single or multiple station metastases (Table 4).

DISCUSSION

In this study, pN(+)/LI(−) patients had a better prognosis than pN(+)/LI(+) patients, whereas there were no significant differences in the RFS between pN(+)/LI(−) and pN(−)/LI(+) clinical stage IA lung adenocarcinoma patients at the participating institutions. LI status, which is

TABLE 2. Univariate log-rank analysis of recurrence-free survival (RFS) and overall survival (OS) according to various factors in patients with lung adenocarcinoma

	All		Node negative		Node positive	
Pathologic variable	**3-y RFS rate (%)**	***P* value**	**3-y RFS rate (%)**	***P* value**	**3-y RFS rate (%)**	***P* value**
LC ratio						
≥30	95.2	<.0001	95.9	<.0001	57.1	.93
<30	78.2		81.4		60.5	
Lymphatic invasion						
Negative	93.1	<.0001	93.4	<.0001	84.6	.059
Positive	63.7		70.8		47.9	
Blood vessel invasion						
Negative	93.1	<.0001	94.3	<.0001	58.8	.93
Positive	63.7		71.0		60.6	
Pleural invasion						
Negative	93.1	<.0001	92.6	<.0001	57.1	.42
Positive	68.6		74.6		65.6	
Lymph node metastasis						
Negative	90.9	<.0001	90.9	—	—	—
Positive	59.9		—		59.9	
	All		**Node negative**		**Node positive**	
	3-y OS rate (%)	***P* value**	**3-y OS rate (%)**	***P* value**	**3-y OS rate (%)**	***P* value**
LC ratio						
≥30	97.0	<.0001	97.3	<.0001	75.0	.76
<30	90.9		92.0		84.5	
Lymphatic invasion						
Negative	96.6	<.0001	96.7	<.0001	92.3	.490
Positive	83.5		85.1		75.0	
Blood vessel invasion						
Negative	96.4	<.0001	96.7	<.0001	88.2	.55
Positive	86.5		88.1		81.0	
Pleural invasion						
Negative	94.9	.0042	95.9	<.0001	100.0	.29
Positive	92.7		91.2		77.3	
Lymph node metastasis						
Negative	95.5	<.0001	95.5	—	—	—
Positive	83.6		—		83.6	

LC, Lepidic component; *RFS*, recurrence-free survival; *OS*, overall survival.

not always positive in N+ patients, is a significant predictive factor in patients with pathologic lymph node metastasis, whereas the lymph node metastasis status is a strong prognostic factor in patients with clinical T1 N0 M0 lung adenocarcinoma.

It is reasonable that lymph node metastasis occurs after cancer cells invade the lymphatic vessels around the tumors; however, 13 of 41 (31.7%) patients with lung adenocarcinoma, whose LI status was negative, exhibited metastasis to regional lymph nodes. One possible explanation is the difficulty in examining all slices of a specimen; some of the slices, including the tumor, could be pathologically assessed. This could be missed if tumors had only slight LI, and the LI status would be determined as negative. Therefore, "no pathologic LI" could either mean no massive LI, just a slight invasion, or it could mean that there was indeed no LI. This is especially the case in pN+ patients, where "no pathologic LI" indicates a slight LI. Slight invasion means the initial period of lymphatic vessel invasion and lymph node metastasis; therefore, patients with slight invasion had a better prognosis than those with massive invasion after complete surgical resection. In pN+ patients the N1 rate was higher in pN(+)/LI(−) patients compared with pN(+)/LI(+) patients, albeit nonsignificantly so. This suggests that pN(+)/LI(−) is indicative of initial lymph node metastasis, as described above.

In pN+ patients, the N2:N1 ratio was higher in pN(+) LI(+) than pN(+)LI(−) patients, although the difference was not statistically significant. The number of pN+ patients was too small to draw any conclusion; however, the tumors that showed massive LI had a higher tendency to progress to N2 disease than LI(−) tumors. Patients with

TABLE 3. Multivariate Cox regression analysis of recurrence-free survival according to various factors

	All		Node negative		Node positive	
Pathologic variables	HR	*P* value	HR	*P* value	HR	*P* value
LC ratio	0.44	.010	0.39	.008	1.7	.62
>30 vs <30	0.23-0.82		0.20-0.78		0.44-6.3	
Lymphatic invasion	2.5	.001	1.9	.045	6.1	.037
Positive vs negative	1.4-4.3		1.0-3.5		1.3-28.7	
Blood vessel invasion	1.8	.037	2.0	.031	0.87	.61
Positive vs negative	1.0-3.1		1.1-3.8		0.31-2.4	
Pleural invasion	1.6	.11	2.1	.024	0.47	.19
Positive vs negative	0.91-2.7		1.1-3.9		0.14-1.5	
Lymph node metastasis	1.9	.032	—*	—*	—*	—*
Positive vs negative	1.1-3.4					

LC, Lepidic component; *HR*, hazard ratio. *Not calculated.

micrometastatic disease to the lymph nodes have been demonstrated to have a worse prognosis than patients with lymph nodes completely replaced by tumors.[15] This suggests that the continuum from LI to lymph node micrometastasis to lymph node replacement might be more complex than previously believed.

As in previous reports, in all patients, multivariate analysis of RFS revealed a lower LC ratio, positive status of lymph nodes, LI, blood vessel invasion, pleural invasion and were poor prognostic factors as well as N+ status in this study.[16,17] In contrast, all evaluated pathologic variables, except for LI status, did not show potential as predictive factors for patients with lymph node involvement. Although lymphatic metastasis status was a strong prognostic factor, LI status was also a significant predictive factor of prognosis in patients with clinical stage IA lung adenocarcinoma. In pN+ patients, LI status had no association with either the clinical or pathologic findings. Thus, the above findings strongly support the significance of LI status as a predictive factor, particularly in patients whose lymph node status is clinically negative and pathologically positive. That is, poor prognosis should be defined according to not only lymph node status but also LI status. Other unknown factors may more precisely determine the true patient population with a poor prognosis. Although pN+ patients typically receive adjuvant chemotherapy, such patients may be classified into no-adjuvant, mild-adjuvant, and severe-adjuvant groups using several predictive factors, including LI status.

Two previous reports have demonstrated that LI status is a poor prognostic factor in surgically resected non–small cell lung cancer[18,19] and a similar result was shown in pathologic stage I or adenocarcinoma patients. Additionally, LI status has been demonstrated to be a prognostic factor regardless of lymph node status.[18,19] However, these previous studies had some limitations; 1 was the quality of LI status evaluation. LI status was evaluated using D2-40 immunostaining in this study, whereas only some tumors were assessed for LI status using D2-40 in the report[19] and the other did not distinguish LI from blood vessel invasion.[18] Thus, the quality of LI evaluation was higher in our study. Another limitation is heterogeneity of the cohort. The analysis was performed only in pathologic stage I patients in the previous studies to minimize heterogeneity.[18,19] However, that analysis of pathologic stage I patients could not assess LI status in pN+ patients. In our study, we evaluated LI status with little heterogeneity in pN+ patients because we included only clinical stage IA adenocarcinoma patients having little heterogeneity.

The rate of lymph node involvement was 6.7% of clinical stage IA lung adenocarcinoma patients in our study (41 out of 609 cases). PET/CT examination has been shown to provide the most accurate preoperative diagnosis[1,4] and results in appropriate treatment. However, a new diagnostic method is necessary to evaluate more accurately the preoperative status of patients with clinical stage IA adenocarcinoma and pathologic lymph node involvement whose preoperative diagnostic modality included a PET scan.

Few patients had lymph node metastasis in clinical stage IA lung adenocarcinoma, which represents one of the main limitations of this study; only a very small number of patients with lymph node involvement had a negative LI status. This makes it difficult to conclude that the prognosis of pN(+)LI(–) patients is equivalent to that of pN(–) LI(+) patients; however, it cannot be denied that LI status plays an important role in assessing patients with lymph node metastasis. The lack of data about pathologic tumor size or morbidity are also limitations of our study. Another is that detailed numbers on patients who received postoperative chemotherapy were not available. Postoperative chemotherapy was performed when pathologic upstaging or recurrence was detected. Additionally, although the follow-up time was too short to assess OS in this study, the OS curves showed similar tendencies to RFS. Because a previous study reported that RFS could be a surrogate

TABLE 4. Clinicopathologic findings in patients with clinical stage IA but pathologic lymph node positive lung adenocarcinoma, according to lymphatic invasion status

Finding	Lymph node metastasis positive: Lymphatic invasion negative (n = 13)	Lymph node metastasis positive: Lymphatic invasion positive (n = 28)	*P* value
Age			
Median	64	66	.96
Interquartile range	56-72	55.25-73.25	
Sex			
Female	4	15	.20
Male	9	13	
CEA			
Median	3.7	3.4	.81
Interquartile range	2.5-4.075	2.65-4.25	
Size*			
Median	2	2.2	.62
Interquartile range	1.6-2.6	1.775-2.5	
GGO† ratio			
Median	0	0	.75
Interquartile range	0-10	0-2.5	
SUV max			
Median	3.4	3.7	.87
Interquartile range	2.7-4.0	2.175-4.925	
LC ratio			
Median	10	10	.16
Interquartile range	10-20	0-12.5	
Blood vessel invasion			
Negative	7	10	.32
Positive	6	18	
Pleural invasion			
Negative	11	18	.28
Positive	2	10	
Lymph node metastasis			
N1	9	11	.18
Single station N2 or single station N2 + N1	2	11	
Multistation N2	2	6	

CEA, Carcinoembryonic antigen; *GGO*, ground-glass opacity; *SUV*, standardized uptake value; *LC*, lepidic component. *Tumor size on the high-resolution computed tomography scan. †GGO ratio on the high-resolution computed tomography scan.

for OS,[20] to evaluate RFS may effectively be equivalent to assessing OS in identifying prognostic factors.

CONCLUSIONS

LI was not always present in pN+ adenocarcinoma patients. In addition, pN(+)LI(−) patients had a better prognosis than pN(+)LI(+) patients, whereas there was no significant difference in RFS between pN(+)LI(−) and pN(−)LI(+) patients with clinical stage IA lung adenocarcinoma. LI status was indicated to classify clinical T1 N0 M0 lung adenocarcinoma patients with and without lymph node involvement into good and poor prognosis groups, the preoperative staging of which conducted using high-resolution CT and FDG-PET/CT. LI status may affect the selection of patients who have to receive adjuvant therapy.

References

1. Lardinois D, Weder W, Hany TF, Kamel EM, Korom S, Seifert B, et al. Staging of non-small-cell lung cancer with integrated positron-emission tomography and computed tomography. *N Engl J Med*. 2003;348:2500-7.
2. Okada M, Nakayama H, Okumura S, Daisaki H, Adachi S, Yoshimura M, et al. Multicenter analysis of high-resolution computed tomography and positron emission tomography/computed tomography findings to choose therapeutic strategies for clinical stage IA lung adenocarcinoma. *J Thorac Cardiovasc Surg*. 2011;141:1384-91.
3. Tsutani Y, Miyata Y, Nakayama H, Okumura S, Adachi S, Yoshimura M, et al. Prediction of pathologic node-negative clinical stage IA lung adenocarcinoma for optimal candidates undergoing sublobar resection. *J Thorac Cardiovasc Surg*. 2012;144:1365-71.
4. Shim SS, Lee KS, Kim BT, Chung MJ, Lee EJ, Han J, et al. Non-small cell lung cancer: prospective comparison of integrated FDG PET/CT and CT alone for preoperative staging. *Radiology*. 2005;236:1011-9.
5. Kim BT, Lee KS, Shim SS, Choi JY, Kwon OJ, Kim H, et al. Stage T1 non-small cell lung cancer: preoperative mediastinal nodal staging with integrated FDG PET/CT—a prospective study. *Radiology*. 2006;241:501-9.
6. Yi CA, Lee KS, Kim BT, Shim SS, Chung MJ, Sung YM, et al. Efficacy of helical dynamic CT versus integrated PET/CT for detection of mediastinal nodal metastasis in non-small cell lung cancer. *AJR Am J Roentgenol*. 2007;188:318-25.
7. Lee SM, Park CM, Paeng JC, Im HJ, Goo JM, Lee HJ, et al. Accuracy and predictive features of FDG-PET/CT and CT for diagnosis of lymph node metastasis of T1 non-small-cell lung cancer manifesting as a subsolid nodule. *Eur Radiol*. 2012;22:1556-63.
8. Goldstraw P, Crowley J, Chansky K, Giroux DJ, Groome PA, Rami-Porta R, et al. The IASLC Lung Cancer Staging Project: proposals for the revision of the TNM stage groupings in the forthcoming (seventh) edition of the TNM Classification of malignant tumours. *J Thorac Oncol*. 2007;2:706-14.
9. Suzuki K, Koike T, Asakawa T, Kusumoto M, Asamura H, Nagai K, et al. A prospective radiological study of thin-section computed tomography to predict pathological noninvasiveness in peripheral clinical IA lung cancer (Japan Clinical Oncology Group 0201). *J Thorac Oncol*. 2011;6:751-6.
10. Travis WD, Brambilla E, Muller-Hermelink HK, Harris CC. Pathology and genetics tumors of the lung, pleura, thymus and heart. In: World Health Organization classification of tumours. Lyon, France: IARC Press; 2004.
11. Nakayama H, Okumura S, Daisaki H, Kato Y, Uehara H, Adachi S, et al. Value of integrated positron emission tomography revised using a phantom study to evaluate malignancy grade of lung adenocarcinoma: a multicenter study. *Cancer*. 2010;116:3170-7.
12. Delbeke D, Coleman RE, Guiberteau MJ, Brown ML, Royal HD, Siegel BA, et al. Procedure guideline for tumor imaging with 18F-FDG PET/CT 1.0. *J Nucl Med*. 2006;47:885-95.
13. Li L, Ren S, Zhang Y, Guan Y, Zhao J, Liu J, et al. Risk factors for predicting the occult nodal metastasis in T1-2N0M0 NSCLC patients staged by PET/CT: potential value in the clinic. *Lung Cancer*. 2013;81:213-7.
14. Kanda Y. Investigation of the freely available easy-to-use software 'EZR' for medical statistics. *Bone Marrow Transplant*. 2013;48:452-8.
15. Riquet M, Bagan P, Le Pimpec Barthes F, Banu E, Scotte F, Foucault C, et al. Completely resected non-small cell lung cancer: reconsidering prognostic value and significance of N2 metastases. *Ann Thorac Surg*. 2007;84:1818-24.
16. Funai K, Sugimura H, Morita T, Shundo Y, Shimizu K, Shiiya N. Lymphatic vessel invasion is a significant prognostic indicator in stage IA lung adenocarcinoma. *Ann Surg Oncol*. 2011;18:2968-72.
17. Kudo Y, Saji H, Shimada Y, Nomura M, Matsubayashi J, Nagao T, et al. Impact of visceral pleural invasion on the survival of patients with non-small cell lung cancer. *Lung Cancer*. 2012;78:153-60.
18. Higgins KA, Chino JP, Ready N, D'Amico TA, Berry MF, Sporn T, et al. Lymphovascular invasion in non-small-cell lung cancer: implications for staging and adjuvant therapy. *J Thorac Oncol*. 2012;7:1141-7.
19. Wang J, Wang B, Zhao W, Guo Y, Chen H, Chu H, et al. Clinical significance and role of lymphatic vessel invasion as a major prognostic implication in non-small cell lung cancer: a meta-analysis. *PloS One*. 2012;7:e52704.
20. Gill S, Sargent D. End points for adjuvant therapy trials: has the time come to accept disease-free survival as a surrogate end point for overall survival? *Oncologist*. 2006;11:624-9.

Cancer Science
The official journal of the Japanese Cancer Association JCA

Involvement of homologous recombination in the synergism between cisplatin and poly (ADP-ribose) polymerase inhibition

Kenji Sakogawa,[1,2] Yoshiro Aoki,[1,2] Keizo Misumi,[1,2] Yoichi Hamai,[2] Manabu Emi,[2] Jun Hihara,[2] Lin Shi,[1] Kazuteru Kono,[1] Yasunori Horikoshi,[1] Jiying Sun,[1] Tsuyoshi Ikura,[3] Morihito Okada[2] and Satoshi Tashiro[1,4]

Departments of [1]Cellular Biology, [2]Surgical Oncology, Research Institute for Radiation Biology and Medicine, Hiroshima University, Hiroshima; [3]Department of Mutagenesis, Radiation Biology Center, Kyoto University, Kyoto, Japan

(Received February 27, 2013/Revised July 31, 2013/Accepted August 29, 2013/Accepted manuscript online September 5, 2013/Article first published online October 10, 2013)

Poly (ADP-ribose) polymerase (PARP) plays a critical role in responding to DNA damage, by activating DNA repair pathways responsible for cellular survival. Inhibition of PARP is used to treat certain solid cancers, such as breast and ovarian cancers. However, its effectiveness with other solid cancers, such as esophageal squamous cell carcinoma (ESCC), has not been clarified. We evaluated the effects of PARP inhibition on the survival of human esophageal cancer cells, with a special focus on the induction and repair of DNA double-strand breaks. The effects were monitored by colony formation assays and DNA damage responses, with immunofluorescence staining of γH2AX and RAD51. We found that PARP inhibition synergized with cisplatin, and the cells were highly sensitive, in a similar manner to the combination of cisplatin and 5-fluorouracil (5-FU). Comparable increases in RAD51 foci formation were observed after each combined treatment with cisplatin and either 3-aminobenzamide (3-AB) or 5-FU in three human esophageal cancer cell lines, TE11, TE14, and TE15. In addition, decreasing the amount of RAD51 by RNA interference rendered the TE11 cells even more hypersensitive to these treatments. Our findings suggested that the homologous recombinational repair pathway may be involved in the synergism between cisplatin and either 3-AB or 5-FU, and that 3-AB and 5-FU may similarly modify the cisplatin-induced DNA damage to types requiring the recruitment of RAD51 proteins for their repair. Understanding these mechanisms could be useful for improving the clinical outcome of ESCC patients who suffer from aggressive disease that presently lacks effective treatment options. (*Cancer Sci* 2013; 104: 1593–1599)

Genomic integrity is maintained by the close cooperation of several DNA repair pathways. Any failure in these pathways can lead to unrepaired DNA lesions, which cause cell-cycle arrest and cell death, either directly or following DNA replication during the S phase of the cell cycle.[1,2] Therefore, the therapeutic effects of DNA-damaging agents may be enhanced by the inhibition of DNA repair. This feature makes DNA repair mechanisms a promising target for novel cancer treatment regimens.

In recent years, poly (ADP-ribose) polymerase (PARP) inhibitors have emerged as a novel class of chemotherapeutic agents. An abundant nuclear protein that catalyzes the formation of PAR polymers from NAD^+, PARP is attached primarily to glutamic acid residues on acceptor proteins.[3] It participates in maintaining genomic integrity, as it is a DNA damage-sensing protein that binds to DNA single-strand breaks (SSBs).[4,5] In addition, PARP plays a role in restarting stalled replication forks, by attracting Mre11 to these sites.[6,7] Therefore, the inhibition of PARP generates DNA damage, and the obstructed replication forks can be converted to replication-associated DNA double-strand breaks (DSBs), which lead to cell cycle arrest and cell death unless they are repaired by the homologous recombinational repair pathway (HR).[8,9] Recently, the PARP inhibitors in clinical use have been shown to trap the PARP1 and PARP2 enzymes at damaged DNA.[10] The trapped PARP–DNA complexes are more cytotoxic than the unrepaired SSBs caused by PARP inactivation, as the complexes require other genetic repair pathways, such as postreplication repair and the Fanconi anemia pathway, in addition to HR, for their repair.[10]

Double-strand breaks are potentially lethal, and are generally considered to be the most toxic DNA lesions.[11,12] Direct DSBs are mainly repaired by the non-homologous end joining pathway,[13] whereas replication-associated DSBs are repaired by the HR and related replication repair pathways.[9] The HR and PARP are intricately linked, because the loss of PARP results in an increase in the recombinogenic lesions normally repaired by HR.[14–17] Therefore, tumor cells defective in HR show extremely high sensitivity to PARP inhibitors.[18–24] In addition, it was recently reported that PARP inhibition sensitizes even HR-proficient tumor cells to ionizing radiation or alkylating agents, such as methyl methanesulfonate, when treated in combination for a short time.[25]

Esophageal squamous cell carcinoma (ESCC) is one of the most lethal malignant diseases, especially in the USA and Europe.[26,27] Based on biochemical modulation studies,[28,29] combined therapy with cisplatin and 5-fluorouracil (5-FU) has recently shown encouraging results, by exerting a synergistic cytotoxic effect. However, the clinical outcomes and the overall survival rates of ESCC patients remain poor.[30] The present study was carried out to evaluate the effects of PARP inhibition on the cellular survival and the DNA damage response in human esophageal cancer cells, with a special focus on DSB induction and repair. We found that PARP inhibition synergized with cisplatin, and strongly increased the percentage of cells bearing nuclear foci of RAD51, a key protein in the HR pathway. This combined therapy was as efficient as the combined treatment with cisplatin and 5-FU, as compared to that with each drug alone. Importantly, RAD51 depletion significantly sensitized the cells to these combined treatments. Our data suggested that HR may be involved in the synergism between cisplatin and either a PARP inhibitor or 5-FU in human esophageal cancer cells. In addition, the PARP inhibitor and 5-FU may similarly modify the cisplatin-induced DNA damage to types requiring the recruitment of RAD51 proteins for their repair.

[4]To whom correspondence should be addressed.
E-mail: ktashiro@hiroshima-u.ac.jp

doi: 10.1111/cas.12281

Materials and Methods

Cells and chemicals. Three human esophageal cancer cell lines, TE11, TE14, and TE15, were obtained from the Cell Resource Center for the Biomedical Research Institute of Development, Aging, and Cancer (Tohoku University, Sendai, Japan). Both TE11 and TE14 are moderately differentiated squamous cell carcinomas, and TE15 is a well-differentiated squamous cell carcinoma. These cell lines were routinely grown in RPMI-1640 (Invitrogen, Carlsbad, CA, USA) supplemented with 10% FBS, and incubated at 37°C in a humidified atmosphere of 5% CO_2 in air. The PARP inhibitor 3-aminobenzamide (3-AB) was obtained from Sigma-Aldrich (#A0788; St. Louis, MO, USA). Cisplatin (Nippon Kayaku, Tokyo, Japan) and 5-FU (Kyowa Hakko Kogyo, Tokyo, Japan) were dissolved in PBS at 1 mM.

Detailed experimental procedures are also provided in the supplementary experimental procedures (Data S1).

Results

Inhibition of PARP in ESCC cell lines. To examine whether PARP inhibition could be efficacious in the treatment of ESCC, we first tested three ESCC cell lines, TE11, TE14, and TE15, for their sensitivity to PARP inhibition. We confirmed the inactivation of PARP by a PARP inhibitor, 3-AB, and the depletion of PARP1 by siRNAs, using immunoblotting analyses (Figs S1,S2A), and then measured the cell viability by a colony formation assay. This assay showed that 3-AB did not decrease the viability of these ESCC cells, as compared to the untreated controls (Fig. 1a).

As PARP inhibition increases the collapse of unresolved SSBs into DSBs at replication forks,[31,32] we investigated the induction of DSBs by PARP inhibition in these ESCC cells. Thus, we carried out immunofluorescence staining for γH2AX, as a marker of DSBs, after the treatment of the ESCC cell lines with 3-AB. As a result, mild increases in the percentages of γH2AX foci-positive cells were observed in all of these cells after the 3-AB treatment (Figs 1b–d,S3A). As the inhibition of PARP by 3-AB treatment did not impair the colony forming activity, most of the DSBs generated by the PARP inhibition might be exactly repaired, and thus not induce cell cycle arrest or cell death. This notion was supported by similar findings obtained by experiments using PARP1-depleted cells in place of 3-AB treatment (Fig. S2A,B).

Combination of PARP inhibition with cisplatin or 5-FU in ESCC cell lines. Cisplatin and 5-FU are effective chemotherapeutic agents used with ESCC patients.[28,29] We wished to examine whether PARP inhibition acts synergistically with either cisplatin or 5-FU against esophageal cancer cells. Thus, we treated TE11, TE14, and TE15 cells with either cisplatin or 5-FU, with or without the inhibition of PARP, and then carried out a colony formation assay to assess the cellular survival after these treatments (Fig. S4). The colony assay revealed that 3-AB sensitized all of these cell lines to cisplatin (Fig. 2a). The synergistic inhibition of cell growth was observed by the combined treatment of TE11 cells with 5 μM cisplatin and 5 mM 3-AB (Fig. S5, Combination Index = 0.471). In stark contrast, no synergism between 3-AB and 5-FU was observed (Fig. 2a).

To explore the reason for this distinct sensitization of cells to cisplatin and 5-FU by 3-AB, we next studied the levels of γH2AX focus formation generated by each treatment. The combined treatment with cisplatin and 3-AB induced significantly higher percentages of γH2AX focus formation compared to the single treatment with cisplatin (Figs 2b,c,S3A). The γH2AX focus formation of TE11 cells peaked at 24 h, and 60% of cells remained foci-positive even at 48 h after treatment (Fig. 2d). Combined treatment with 5-FU and 3-AB induced γH2AX focus formation with similar increases and kinetics as the single treatment with 5-FU, and it peaked at 24 h after treatment (Figs 2b,c,e,S3A). Although the TE15 cells treated with 5-FU and 3-AB showed a lower percentage of γH2AX foci-positive cells, as compared to the 5-FU single treatment, the average numbers of γH2AX foci per cell generated by these treatments were similar to those of the other cell lines (Figs 2b,S3A). Similar findings were obtained by the depletion of PARP1 using siRNA, instead of 3-AB treatment (Fig. S2C). Therefore, the significantly increased induction of DSBs by PARP inhibition could

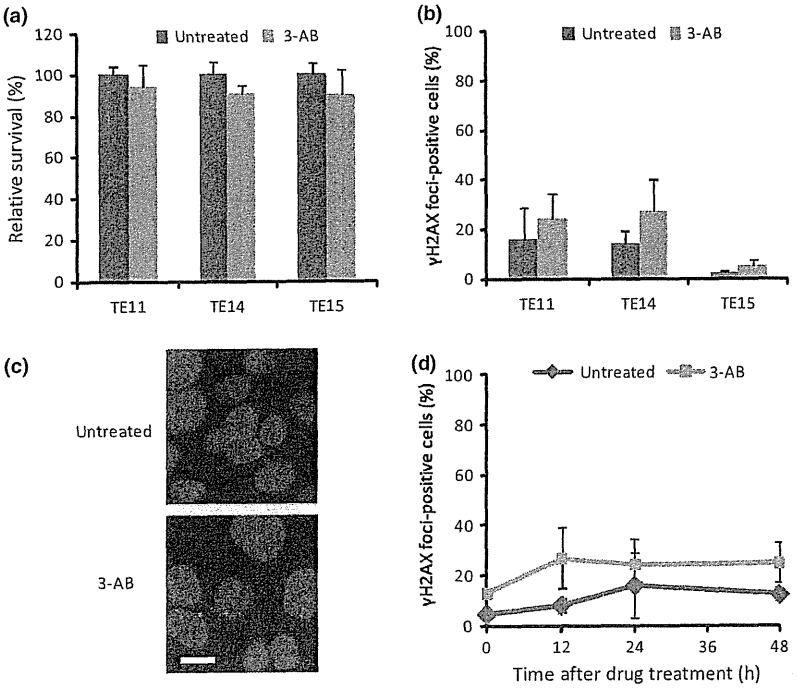

Fig. 1. Poly (ADP-ribose) polymerase (PARP) inhibition by 3-aminobenzamide (3-AB) in human esophageal cancer cell lines. (a) Survival of TE11, TE14, and TE15 cells after treatment with 3-AB. (b) Induction of double-strand breaks, indicating γH2AX focus formation, at 24 h after PARP inhibition by 3-AB in TE11, TE14, and TE15 cells. (c) DNA (blue) and γH2AX foci (red) were visualized at 24 h after treatment of TE11 cells. Scale bar = 10 μm. (d) Kinetics of γH2AX foci formation at the indicated periods up to 48 h, after 3-AB pretreatment for 48 h. Cells with 10 or more foci were counted as positive. At least 200 nuclei were counted for each experiment. The average and SD from at least three experiments are shown.

doi: 10.1111/cas.12281

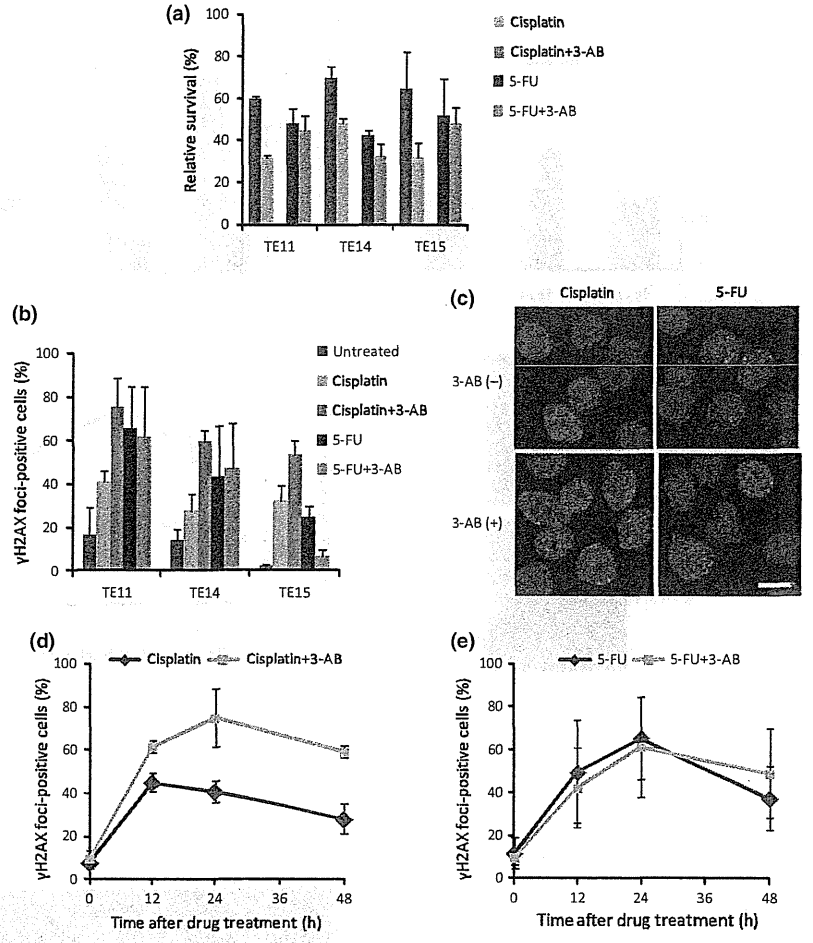

Fig. 2. Combination of a poly (ADP-ribose) polymerase (PARP) inhibitor 3-aminobenzamide (3-AB) with cisplatin or 5-fluorouracil (5-FU) in human esophageal cancer cell lines. (a) Survival of TE11, TE14, and TE15 cells after treatment with either 5 μM cisplatin for 1 h or 3 μM 5-FU for 24 h, with or without pretreatment with 3 mM (TE14) or 5 mM (TE11 and TE15) 3-AB for 48 h. (b) Evaluation of the γH2AX focus formation at 24 h after treatment of TE11, TE14, and TE15 cells with either cisplatin or 5-FU, with or without pretreatment with 3-AB. (c) DNA (blue) and γH2AX foci (red) were visualized at 24 h after treatment of TE11 cells. Scale bar = 10 μm. (d,e) TE11 cells were treated with either cisplatin or 5-FU, with or without pretreatment with 3-AB. Cells with 10 or more foci were counted as positive. At least 200 nuclei were counted for each experiment. The average and SD from at least three experiments are shown.

enhance the cytotoxic effects of cisplatin treatment of these ESCC cells.

Modulation of ESCC cell sensitivity to combined treatment with cisplatin and 5-FU by PARP inhibition. Having established that the PARP inhibitor could sensitize ESCC cells to cisplatin, we next compared the anticancer effects between the combined treatments with cisplatin/3-AB and cisplatin/5-FU, the most standard chemotherapy for ESCC. We treated the ESCC cells with cisplatin and 5-FU in concurrent combinations, and then measured the cell viability by a colony formation assay. As a result, all of the ESCC cell lines treated with cisplatin plus 5-FU showed similar high degrees of sensitivity to the cisplatin plus PARP inhibition (Figs 2a,3a,S2B).

To clarify the reason for the high sensitivity of the ESCC cells to the combined treatment with cisplatin and 5-FU, we next carried out an immunofluorescence assay for γH2AX proteins in these cell lines. This assay revealed that the γH2AX focus formation following the cisplatin plus 5-FU treatment was quite consistent with that following the cisplatin plus 3-AB treatment (Figs 2b,d,3b,d,S3A). Thus, we hypothesized that 3-AB and 5-FU might play analogous roles in the increased numbers of DSBs formed in combination with cisplatin, resulting in the similar sensitivities of the cells to combined treatments with cisplatin and either 3-AB or 5-FU.

To confirm our hypothesis, we next investigated the cytotoxic effect of the triple combination of 3-AB, cisplatin, and 5-FU against ESCC cells. First, we inhibited PARP by 3-AB or depleted it by siRNAs, and then treated the cells concurrently with cisplatin and 5-FU. The cellular survival was confirmed by a colony formation assay. This assay showed that the triple treatment did not cause a further decrease in the survival of the cells, as compared to the combined treatment with cisplatin and either 3-AB or 5-FU (Figs 2a,3a).

Next, we examined the γH2AX focus formation, to assess the induction of DSBs by the triple treatment of the ESCC cells. Immunofluorescence staining analysis of γH2AX revealed that the level of γH2AX focus formation induced by the triple treatment was not significantly different from that induced by the combined treatment with cisplatin and either 3-AB or 5-FU in these cells (Figs 2b–d,3b–d,S3A). Similar findings were obtained by PARP1 depletion instead of 3-AB treatment (Fig. S2B,C). Therefore, these findings indirectly supported our hypothesis that PARP inhibition and 5-FU increase the sensitivity of ESCC cells to cisplatin, by disturbing the same pathway involving the induction or repair of DNA damage.

Validation of HR, indicating RAD51 foci formation in ESCC cells. Poly (ADP-ribose) polymerase inhibition induces DSBs, which require HR for their repair.[31,32] Thus, we next examined the involvement of HR after the induction of DSBs by PARP inhibition, to understand the mechanisms underlying the synergism between cisplatin and either 3-AB or 5-FU in ESCC cells. We assessed RAD51 focus formation, as a hallmark of ongoing HR, after treatments with 3-AB, cisplatin, and 5-FU alone and in combination.

Immunofluorescence staining of RAD51 revealed that the 3-AB treatment significantly increased the percentage of cells with RAD51 foci, as compared to the untreated controls (Figs 4a–c,S3B). As 3-AB did not disturb the colony formation

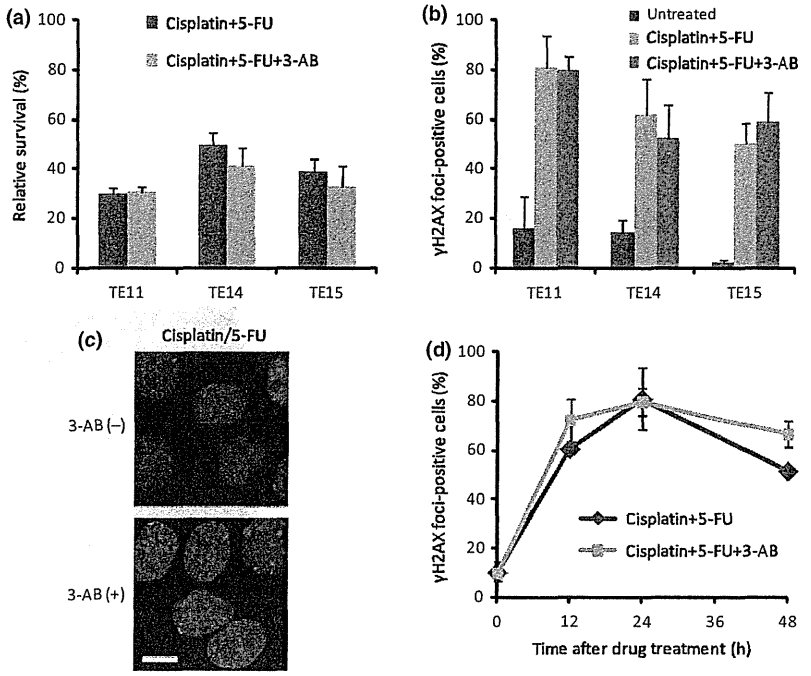

Fig. 3. Comparison of standard combined treatments for esophageal squamous cell carcinoma using cisplatin and 5-fluorouracil (5-FU) with or without poly (ADP-ribose) polymerase (PARP) inhibition . (a) Survival of TE11, TE14, and TE15 cells after concurrent combined treatments with cisplatin and 5-FU, with or without pretreatment with 3-aminobenzamide (3-AB). (b) Evaluation of the γH2AX focus formation at 24 h after combined treatment of TE11, TE14, and TE15 cells with cisplatin and 5-FU, with or without a pretreatment with 3-AB. (c) DNA (blue) and γH2AX foci (red) were visualized at 24 h after treatment of TE11 cells. Scale bar = 10 μm. (d) TE11 cells were treated with cisplatin and 5-FU in concurrent combination, after pretreatment with 3-AB. Cells with 10 or more foci were counted as positive. At least 200 nuclei were counted for each experiment. The average and SD from at least three experiments are shown.

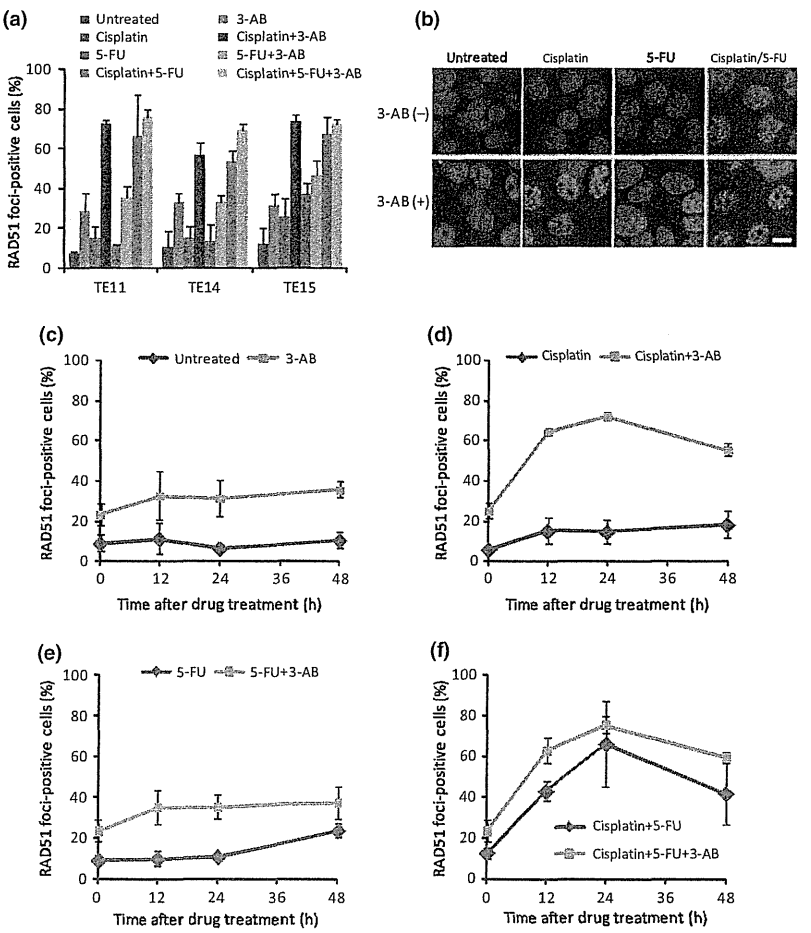

Fig. 4. Validation of the homologous recombinational repair pathway in esophageal squamous cell carcinoma cells, indicating RAD51 focus formation. (a) Evaluation of the RAD51 focus formation 24 h after treatment of TE11, TE14, and TE15 cells with cisplatin or 5-fluorouracil (5-FU) alone and in combination, with or without a pretreatment with 3-aminobenzamide (3-AB). (b) Representative images of DNA (blue) and RAD51 foci (green) 24 h after the treatment of TE11 cells. Scale bar = 10 μm. (c) TE11 cells were treated with or without 3-AB. (d,e) TE11 cells were treated with either cisplatin or 5-FU, with or without pretreatment with 3-AB. (f) TE11 cells were treated concurrently with cisplatin and 5-FU, after pretreatment with 5 mM 3-AB for 48 h. Cells with five or more foci were counted as positive. At least 200 nuclei were counted for each experiment. The average and SD from three experiments are shown.

doi: 10.1111/cas.12281

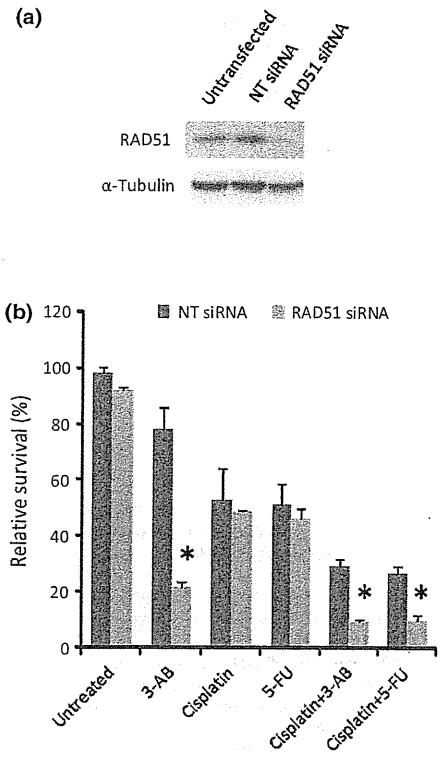

Fig. 5. Knockdown of RAD51 protein renders esophageal squamous cell carcinoma TE11 cells hypersensitive to combinations of cisplatin and either 3-aminobenzamide (3-AB) or 5-fluorouracil (5-FU). (a) Immunoblotting analysis of RAD51 (top) and α-tubulin (bottom) in TE11 cells, after RAD51 siRNA or non-targeting (NT) siRNA depletion for 24 h. (b) Relative survival of TE11 cells treated with 3-AB, cisplatin, and 5-FU alone and in combination, under the same experimental conditions after RAD51 siRNA or NT siRNA depletion for 24 h, confirmed by colony formation assay. The average and SD from at least three experiments are shown. Values marked with asterisks are statistically significant, as compared with each control (*$P < 0.05$).

activity of the ESCC cells (Fig. 1a), this finding suggested that the 3-AB-induced DNA damage might be exactly repaired by HR.

The treatment of cells with cisplatin or 5-FU alone caused only a slight increase in the percentage of RAD51 foci-positive cells up to 48 h after treatment. However, the combined treatment of these cells with cisplatin and either 3-AB or 5-FU markedly increased the percentage of cells with RAD51 foci, which reached a maximum at 24 h after each treatment (Figs 4,S3B). When used in combination with cisplatin, both 3-AB and 5-FU vigorously promoted the production of DSBs, which require the recruitment of RAD51 proteins for their repair in these ESCC cells.

The PARP-inhibited ESCC cells treated with or without 5-FU showed similar levels of RAD51 focus formation after each treatment (Figs 4a–c,e,S3B). Moreover, the addition of 5-FU did not change the kinetics of RAD51 focus formation by the combined treatment with cisplatin and 3-AB (Figs 4a,b,d,f, S3B). These data suggested that 5-FU might not affect the RAD51 focus formation induced by 3-AB, with or without cisplatin, in these ESCC cells. Similar results were obtained by the depletion of PARP1 in place of 3-AB treatment (Fig. S2D). Thus, the validation of HR additionally supported our hypothesis that the enhancement of the anticancer effect of cisplatin, by either PARP inhibition or 5-FU, might be attributed to similar mechanisms involving HR repair in ESCC cells.

Depletion of RAD51 enhances 3-AB- or 5-FU-mediated sensitization of ESCC cells to cisplatin. As RAD51 plays crucial and well-established roles in HR,[33–35] we hypothesized that the critical role of HR would be the underlying reason for the synergistic effect of cisplatin and either 3-AB or 5-FU in ESCC cells. Thus, we examined how RAD51 depletion affected the sensitivity of TE11 cells to these combined treatments. The depletion of RAD51 by siRNAs was confirmed by an immunoblotting analysis, using anti-RAD51 antibodies (Figs 5a,S6A).

We treated RAD51-knockdown cells with either 3-AB, cisplatin, and 5-FU alone or in combination, under the same experimental conditions as described above, and then the cellular survival was measured by a colony formation assay (Figs 5b,S6B). As expected, RAD51 depletion caused a drastic increase in the cellular sensitivity to 3-AB. In contrast, RAD51 knockdown showed neither a synergistic nor an additive effect on the sensitivity to cisplatin or 5-FU alone (Figs 5b,S6B). These findings suggested that HR might play a major role in the repair of DNA damage induced by treatment with 3-AB, but not with cisplatin or 5-FU alone. In contrast to the treatment with cisplatin or 5-FU alone, RAD51 repression significantly sensitized the TE11 cells to cisplatin in combination with either 3-AB or 5-FU. Considering our finding that the addition of 3-AB to treatment with 5-FU or cisplatin/5-FU did not enhance the γH2AX focus formation (Figs 2b,e,3b,d,S3A), these data supported our hypothesis that the conversion of cisplatin-induced DNA damage to the types requiring HR for their repair could play an important role in TE11 cells sensitization to cisplatin by both 3-AB and 5-FU.

Discussion

Our data showed that the inhibition of PARP exerts a synergistic tumor-cell killing effect in combination with cisplatin, but not 5-FU, against three ESCC cell lines, TE11, TE14, and TE15, by the increased induction of DNA damage requiring HR for repair. Moreover, in the sensitization of cells to cisplatin, PARP inhibition by 3-AB and 5-FU may function by similar mechanisms involving HR.

Poly (ADP-ribose) polymerase inhibitors were originally developed to selectively target HR-defective cells, and have been tested as a monotherapy and in combination with an alkylating agent and cisplatin in patients with certain solid tumors.[36–39] In this study, 3-AB, as a single agent, had minimal cytotoxic efficacy (Fig. 1a), and only modest increases of γH2AX and RAD51 focus formation in response to 3-AB were observed in the ESCC cells, as compared to the untreated controls (Figs 1b,4a). These data indicated that the DSBs induced by 3-AB may be exactly repaired by HR, and therefore, these cells are predicted to be proficient in HR repair.[40] Thus, consistent with a previous study,[25] PARP inhibitors, in combination with certain DNA damaging agents, could be useful in the treatment of even HR-proficient cancer cells.

Poly (ADP-ribose) polymerase and RAD51 are required to reactivate replication at stalled DNA forks.[6,7,41,42] Therefore, the synergism between cisplatin and either 3-AB or 5-FU may be similarly attributed to the failure of replication reactivation at stalled replication forks, due to the inhibition of PARP activity or the incorporation of 5-FU into replicating DNA in the cisplatin-induced DNA lesions. This failure may lead to increased RAD51 focus formation, for the efficient restarting of stalled replication forks by HR. The addition of 3-AB to either the 5-FU or cisplatin/5-FU treatment neither facilitated nor repressed the cellular survival and γH2AX/RAD51 focus formation (Figs 2a,b,3a,b,4a), therefore, 3-AB and 5-FU may function in an epistatic pathway for the cisplatin-induced DNA lesion repair in ESCC cells. Our results suggested that a novel regimen, combining cisplatin with a PARP inhibitor, may have

similar efficacy to the standard combined chemotherapy of cisplatin and 5-FU in the treatment of ESCC patients.

In conclusion, we have shown that HR may be involved in the synergism between cisplatin and either PARP inhibition or 5-FU treatment, in human esophageal cancer cell lines. Our findings provide a platform for extending the potential use of PARP inhibitors to ESCC patients. Poly (ADP-ribose) polymerase inhibitors could be novel combinational counterparts of cisplatin in the treatment of ESCC. Moreover, cancer cells with decreased RAD51 activity, due to mutations or dysregulation, would be more sensitive to PARP inhibitors than the surrounding HR-proficient tissue.[43,44] Therefore, considering the therapeutic potential of PARP inhibitors in the treatment of ESCC, such cases would be ideal candidates for PARP inhibitor therapy, and the side-effects usually seen with classical cytotoxic anticancer drugs could be minimized. Although it may be premature to extrapolate our results from only three cultured cell lines, further investigations of the mechanisms responsible for the increases of RAD51 foci, in combination with cisplatin and either PARP inhibition or 5-FU treatment, in human cancer cells will provide novel insights into cancer therapies.

Acknowledgment

This work was supported by the Grants-in-Aid Program from the Ministry of Education, Culture, Sports, Science and Technology of Japan.

Disclosure Statement

The authors have no conflict of interest.

References

1 Hoeijmakers JH. Genome maintenance mechanisms for preventing cancer. *Nature* 2001; **411**: 366–74.
2 Farmer H, McCabe N, Lord CJ *et al.* Targeting the DNA repair defect in BRCA mutant cells as a therapeutic strategy. *Nature* 2005; **434**: 917–21.
3 Satoh MS, Lindahl T. Role of poly (ADP-ribose) formation in DNA repair. *Nature* 1992; **356**: 356–8.
4 Lindahl T, Satoh MS, Poirier GG, Klungland A. Post-translational modification of poly (ADP-ribose) polymerase induced by DNA strand breaks. *Trends Biochem Sci* 1995; **20**: 405–11.
5 D'Amours D, Desnoyers S, D'Silva I, Poirier GG. Poly(ADP-ribosyl)ation reactions in the regulation of nuclear functions. *Biochem J* 1999; **342**: 249–68.
6 Bryant HE, Petermann E, Schultz N *et al.* PARP is activated at stalled forks to mediate Mre11-dependent replication restart and recombination. *EMBO J* 2009; **28**: 2601–15.
7 Yang YG, Cortes U, Patnaik S, Jasin M, Wang ZQ. Ablation of PARP-1 does not interfere with the repair of DNA double-strand breaks, but compromises the reactivation of stalled replication forks. *Oncogene* 2004; **23**: 3872–82.
8 Schultz N, Lopez E, Saleh-Gohari N, Helleday T. Poly (ADP-ribose) polymerase (PARP-1) has a controlling role in homologous recombination. *Nucleic Acids Res* 2003; **31**: 4959–64.
9 Arnaudeau C, Lundin C, Helleday T. DNA double-strand breaks associated with replication forks are predominantly repaired by homologous recombination involving an exchange mechanism in mammalian cells. *J Mol Biol* 2001; **307**: 1235–45.
10 Murai J, Huang SY, Das BB *et al.* Trapping of PARP1 and PARP2 by clinical PARP inhibitors. *Cancer Res* 2012; **72**: 5588–99.
11 Hsiang YH, Lihou MG, Liu LF. Arrest of replication forks by drug-stabilized topoisomerase I-DNA cleavable complexes as a mechanism of cell killing by camptothecin. *Cancer Res* 1989; **49**: 5077–82.
12 Markovits J, Pommier Y, Kerrigan D, Covey JM, Tilchen EJ, Kohn KW. Topoisomerase II-mediated DNA breaks and cytotoxicity in relation to cell proliferation and the cell cycle in NIH 3T3 fibroblasts and L1210 leukemia cells. *Cancer Res* 1987; **47**: 2050–5.
13 Sargent RG, Brenneman MA, Wilson JH. Repair of site-specific double-strand breaks in a mammalian chromosome by homologous and illegitimate recombination. *Mol Cell Biol* 1997; **17**: 267–77.
14 Magnusson J, Ramel C. Inhibitor of poly (ADP-ribose)transferase potentiates the recombinogenic but not the mutagenic action of alkylating agents in somatic cells in vivo in *Drosophila melanogaster*. *Mutagenesis* 1990; **5**: 511–4.
15 Waldman AS, Waldman BC. Stimulation of intrachromosomal homologous recombination in mammalian cells by an inhibitor of poly(ADP-ribosylation). *Nucleic Acids Res* 1991; **19**: 5943–7.
16 Schreiber V, Hunting D, Trucco C *et al.* A dominant-negative mutant of human poly (ADP-ribose) polymerase affects cell recovery, apoptosis and sister chromatid exchange following DNA damage. *Proc Natl Acad Sci USA* 1995; **92**: 4753–7.
17 Semionov A, Cournoyer D, Chow TY. Inhibition of poly (ADP-ribose)polymerase stimulates extrachromosomal homologous recombination in mouse Ltk-fibroblasts. *Nucleic Acids Res* 1999; **27**: 4526–31.
18 Donawho CK, Luo Y, Luo Y *et al.* ABT-888, an orally active poly (ADP-ribose) polymerase inhibitor that potentiates DNA-damaging agents in preclinical tumor models. *Clin Cancer Res* 2007; **13**: 2728–37.
19 Penning TD, Zhu GD, Gandhi VB *et al.* Discovery of the Poly (ADP-ribose) polymerase (PARP) inhibitor 2-[(R)-2-methylpyrrolidin-2-yl]-1H-benzimidazole-4-carboxamide (ABT-888) for the treatment of cancer. *J Med Chem* 2009; **52**: 514–23.
20 Evers B, Drost R, Schut E *et al.* Selective inhibition of BRCA2-deficient mammary tumor cell growth by AZD2281 and cisplatin. *Clin Cancer Res* 2008; **14**: 3916–25.
21 Hay T, Matthews JR, Pietzka L *et al.* Poly (ADP-ribose) polymerase-1 inhibitor treatment regresses autochthonous Brca2/p53-mutant mammary tumors in vivo and delays tumor relapse in combination with carboplatin. *Cancer Res* 2009; **69**: 3850–5.
22 Menear KA, Adcock C, Boulter R *et al.* 4-[3-(4-cyclopropanecarbonylpiperazine-1-carbonyl)-4-fluorobenzyl]-2H-phthalazin-1-one: a novel bioavailable inhibitor of poly (ADP-ribose) polymerase-1. *J Med Chem* 2008; **51**: 6581–91.
23 Rottenberg S, Jaspers JE, Kersbergen A *et al.* High sensitivity of BRCA1-deficient mammary tumors to the PARP inhibitor AZD2281 alone and in combination with platinum drugs. *Proc Natl Acad Sci USA* 2008; **105**: 17079–84.
24 Jones P, Altamura S, Boueres J *et al.* Discovery of 2-{4-[(3S)-piperidin-3-yl] phenyl}-2H-indazole-7-carboxamide (MK-4827): a novel oral poly (ADP-ribose)polymerase (PARP) inhibitor efficacious in BRCA-1 and -2 mutant tumors. *J Med Chem* 2009; **52**: 7170–85.
25 Löser DA, Shibata A, Shibata AK, Woodbine LJ, Jeggo PA, Chalmers AJ. Sensitization to radiation and alkylating agents by inhibitors of poly (ADP-ribose) polymerase is enhanced in cells deficient in DNA double-strand break repair. *Mol Cancer Ther* 2010; **9**: 1775–87.
26 Parkin DM, Bray F, Ferlay J, Pisani P. Global cancer statistics, 2002. *CA Cancer J Clin* 2005; **55**: 74–108.
27 Shimada H, Nabeya Y, Okazumi S *et al.* Prediction of survival with squamous cell carcinoma antigen in patients with resectable esophageal squamous cell carcinoma. *Surgery* 2003; **133**: 486–94.
28 Sekiguchi H, Akiyama S, Fujiwara M *et al.* Phase II trial of 5-fluorouracil and low-dose cisplatin in patients with squamous cell carcinoma of the esophagus. *Surg Today* 1999; **29**: 97–101.
29 Scanlon KJ, Newman EM, Lu Y, Priest DG. Biochemical basis for cisplatin and 5-fluorouracil synergism in human ovarian carcinoma cells. *Proc Natl Acad Sci USA* 1986; **83**: 8923–5.
30 Borghesi S, Hawkins MA, Tait D. Oesophagectomy after definitive chemoradiation in patients with locally advanced oesophageal cancer. *Clin Oncol (R Coll Radiol)* 2008; **20**: 221–6.
31 Bryant HE, Schultz N, Thomas HD *et al.* Specific killing of BRCA2-deficient tumours with inhibitors of poly (ADP-ribose) polymerase. *Nature* 2005; **434**: 913–7.
32 Saleh-Gohari N, Bryant HE, Schultz N, Parker KM, Cassel TN, Helleday T. Spontaneous homologous recombination is induced by collapsed replication forks that are caused by endogenous DNA single-strand breaks. *Mol Cell Biol* 2005; **25**: 7158–69.
33 Lim DS, Hasty P. A mutation in mouse rad51 results in an early embryonic lethal that is suppressed by a mutation in p53. *Mol Cell Biol* 1996; **16**: 7133–43.
34 Tsuzuki T, Fujii Y, Sakumi K *et al.* Targeted disruption of the Rad51 gene leads to lethality in embryonic mice. *Proc Natl Acad Sci USA* 1996; **93**: 6236–40.
35 Sonoda E, Sasaki MS, Buerstedde JM *et al.* Rad51-deficient vertebrate cells accumulate chromosomal breaks prior to cell death. *EMBO J* 1998; **17**: 598–608.

doi: 10.1111/cas.12281

36 Turner N, Tutt A, Ashworth A. Hallmarks of "BRCAness" in sporadic cancers. *Nat Rev Cancer* 2004; **4**: 814–9.
37 Vesprini D, Narod SA, Trachtenberg J *et al.* The therapeutic ratio is preserved for radiotherapy or cisplatin treatment in BRCA2-mutated prostate cancers. *Can Urol Assoc J* 2011; **5**: E31–5.
38 Plummer R, Jones C, Middleton M *et al.* Phase I study of the poly (ADP-ribose) polymerase inhibitor, AG014699, in combination with temozolomide in patients with advanced solid tumors. *Clin Cancer Res* 2008; **14**: 7917–23.
39 Rajan A, Carter CA, Kelly RJ *et al.* A phase I combination study of olaparib with cisplatin and gemcitabine in adults with solid tumors. *Clin Cancer Res* 2012; **18**: 2344–51.
40 Mukhopadhyay A, Elattar A, Cerbinskaite A *et al.* Development of a functional assay for homologous recombination status in primary cultures of epithelial ovarian tumor and correlation with sensitivity to poly (ADP-ribose) polymerase inhibitors. *Clin Cancer Res* 2010; **16**: 2344–51.
41 Davies SL, North PS, Hickson ID. Role for BLM in replication-fork restart and suppression of origin firing after replicative stress. *Nat Struct Mol* 2007; **14**: 677–9.
42 Petermann E, Orta ML, Issaeva N, Schultz N, Helleday T. Hydroxyurea-stalled replication forks become progressively inactivated and require two different RAD51-mediated pathways for restart and repair. *Mol Cell* 2010; **37**: 492–502.
43 Rouleau M, Patel A, Hendzel MJ, Kaufmann SH, Poirier GG. PARP inhibition: PARP1 and beyond. *Nat Rev Cancer* 2010; **10**: 293–301.
44 Ashworth A. A synthetic lethal therapeutic approach: poly(ADP) ribose polymerase inhibitors for the treatment of cancers deficient in DNA double-strand break repair. *J Clin Oncol* 2008; **26**: 3785–90.

Supporting Information

Additional supporting information may be found in the online version of this article:

Fig. S1. Immunoblotting analysis of poly (ADP-ribose) PAR and poly (ADP-ribose) polymerase 1 (PARP1) in esophageal squamous cell carcinoma TE11 cells after exposure to 3-aminobenzamide (3-AB).

Fig. S2. Treatment of poly (ADP-ribose) polymerase 1 (PARP1)-depleted esophageal squamous cell carcinoma TE11 cells with anticancer drugs.

Fig. S3. Numbers of γH2AX and RAD51 foci per nucleus after treatment with anticancer drugs.

Fig. S4. Time schedule of treatments with anticancer drugs.

Fig. S5. Dose–response analysis of the survival of esophageal squamous cell carcinoma TE11 cells treated with cisplatin and 3-aminobenzamide (3-AB) in combination.

Fig. S6. Knockdown of RAD51 protein using RAD51 siRNA (#2) also renders TE11 cells hypersensitive to combinations of cisplatin and either 3-aminobenzamide (3-AB) or 5-fluorouracil (5-FU).

Data S1. Supplementary experimental procedures and discussion.

Oncologic outcomes of segmentectomy compared with lobectomy for clinical stage IA lung adenocarcinoma: Propensity score–matched analysis in a multicenter study

Yasuhiro Tsutani, MD, PhD,[a] Yoshihiro Miyata, MD, PhD,[a] Haruhiko Nakayama, MD, PhD,[b] Sakae Okumura, MD, PhD,[c] Shuji Adachi, MD, PhD,[d] Masahiro Yoshimura, MD, PhD,[e] and Morihito Okada, MD, PhD[a]

Objective: Our objective was to compare the oncologic outcomes of lobectomy and segmentectomy for clinical stage IA lung adenocarcinoma.

Methods: We examined 481 of 618 consecutive patients with clinical stage IA lung adenocarcinoma who underwent lobectomy or segmentectomy after preoperative high-resolution computed tomography and F-18-fluorodeoxyglucose positron emission tomography/computed tomography. Patients (n = 137) who underwent wedge resection were excluded. Lobectomy (n = 383) and segmentectomy (n = 98) as well as surgical results were analyzed for all patients and their propensity score–matched pairs.

Results: Recurrence-free survival (RFS) and overall survival (OS) were not significantly different between patients undergoing lobectomy (3-year RFS, 87.3%; 3-year OS, 94.1%) and segmentectomy (3-year RFS, 91.4%; hazard ratio [HR], 0.57; 95% confidence interval [CI], 0.27-1.20; $P = .14$; 3-year OS, 96.9%; HR, 0.49; 95% CI, 0.17-1.38; $P = .18$). Significant differences in clinical factors such as solid tumor size ($P < .001$), maximum standardized uptake value (SUVmax) ($P < .001$), and tumor location (side, $P = .005$; lobe, $P = .001$) were observed between both treatment groups. In 81 propensity score–matched pairs including variables such as age, gender, solid tumor size, SUVmax, side, and lobe, RFS and OS were similar between patients undergoing lobectomy (3-year RFS, 92.9%, 3-year OS, 93.2%) and segmentectomy (3-year RFS, 90.9%; 3-year OS, 95.7%).

Conclusions: Segmentectomy is suitable for clinical stage IA lung adenocarcinoma, with survivals equivalent to those of standard lobectomy. (J Thorac Cardiovasc Surg 2013;146:358-64)

GTS

Segmentectomy for treating small lung cancer has been a topic of debate for a long time. In 1995, the Lung Cancer Study Group conducted a prospective randomized controlled trial comparing limited resection (including segmentectomy and wedge resection) with lobectomy for clinical T1 N0 M0 non–small cell lung cancer (NSCLC). The study concluded that limited resection resulted in higher local recurrence and lower survival.[1] A recent study from the Surveillance Epidemiology and End Results database showed that lobectomy conferred a significant advantage compared with segmentectomy in stage I NSCLC.[2] In contrast, several studies reported that the survivals after segmentectomy and those after lobectomy were similar.[3-7] However, few reports compare between segmentectomy and lobectomy with matched patient variables affecting survival.

Recently, we[8,9] reported that solid tumor size, defined as the maximum dimension of the solid component excluding the ground-glass opacity (GGO) component on high-resolution computed tomography (HRCT), and maximum standardized uptake value (SUVmax) on [18F]-fluoro-2-deoxy-D-glucose positron emission tomography/computed tomography (FDG-PET/CT), are useful for predicting the pathologic invasiveness or prognosis in clinical stage IA lung adenocarcinoma. These preoperative radiologic findings are important when choosing treatment strategies for NSCLC, particularly for lung adenocarcinoma.[8,9]

The purpose of this retrospective study was to compare the oncologic outcomes between lobectomy and segmentectomy in patients with clinical stage IA lung adenocarcinoma, adjusted for preoperative factors including HRCT and FDG-PET/CT findings, to minimize the effect of patient selection bias. Segmentectomy and wedge resection are considerably different procedures for lung cancer; the former can be used to approach hilar lymph nodes and to get sufficient margin, whereas the latter cannot. Therefore, we excluded wedge resection from this study.

From the Department of Surgical Oncology,[a] Hiroshima University, Hiroshima; the Department of Thoracic Surgery,[b] Kanagawa Cancer Center, Yokohama; the Department of Thoracic Surgery,[c] Cancer Institute Hospital, Tokyo; and the Departments of Radiology[d] and Thoracic Surgery,[e] Hyogo Cancer Center, Akashi, Japan.

Disclosures: Authors have nothing to disclose with regard to commercial support.

Received for publication Oct 4, 2012; revisions received Jan 10, 2013; accepted for publication Feb 11, 2013; available ahead of print March 13, 2013.

Address for reprints: Morihito Okada, MD, PhD, Department of Surgical Oncology, Research Institute for Radiation Biology and Medicine, Hiroshima University, 1-2-3-Kasumi, Minami-ku, Hiroshima City, Hiroshima 734-0037, Japan (E-mail: morihito@hiroshima-u.ac.jp).

0022-5223/$36.00

http://dx.doi.org/10.1016/j.jtcvs.2013.02.008

Abbreviations and Acronyms

CI	= confidence interval
FDG-PET/CT	= [18F]-fluoro-2-deoxy-D-glucose positron emission tomography/computed tomography
GGO	= ground-glass opacity
HRCT	= high-resolution computed tomography
NSCLC	= non–small cell lung cancer
OS	= overall survival
RFS	= recurrence-free survival
SUVmax	= maximum standardized uptake value

PATIENTS AND METHODS

Patients

We enrolled 618 patients with clinical T1 N0 M0 stage IA lung adenocarcinoma from 4 institutions (Hiroshima University, Kanagawa Cancer Center, Cancer Institute Hospital, and Hyogo Cancer Center, Japan) between August 1, 2005 and June 30, 2010, to evaluate the significance of FDG-PET/CT. Patients with incompletely resected tumors (R1 or R2) and those with multiple tumors or previous lung operations were not included in the database. The database has been maintained prospectively. The patient data obtained from this multicenter database were retrospectively analyzed in the present study. HRCT and FDG-PET/CT followed by curative R0 resection were performed for all patients staged according to the TNM Classification of Malignant Tumors, seventh edition.[10] Mediastinoscopy or endobronchial ultrasonography was not routinely performed because all patients received preoperative HRCT and FDG-PET/CT; HRCT revealed no swelling of mediastinal or hilar lymph nodes and FDG-PET showed no accumulation in these lymph nodes. Sublobar resection was allowed in cases of complete removal of the disease, using the optional procedure instead of lobectomy for a peripheral T1 N0 M0 tumor. The other patients underwent standard lobectomy. All patients who underwent segmentectomy were suitable for lobectomy and all patients who underwent lobectomy were technically suitable for segmentectomy. Patients who had lymph node metastasis pathologically received platinum-based chemotherapy after operation.

The inclusion criteria were preoperative staging determined by HRCT and FDG-PET/CT, curative surgery without neoadjuvant chemotherapy or radiotherapy, and a definitive histopathologic diagnosis of lung adenocarcinoma. The study was approved by the institutional review boards of the participating institutions; the requirement for informed consent from individual patients was waived because the study was a retrospective review of the patient database. Of the 618 patients, 137 who underwent wedge resection were excluded; the remaining 481 were included in this analysis.

HRCT

Sixteen-row multidetector CT was used to obtain chest images independent of subsequent FDG-PET/CT examinations. For high-resolution images of the tumors, the following parameters were used: 120 kVp, 200 mA, 1- to 2-mm section thickness, 512 × 512-pixel resolution, 0.5- to 1.0-second scanning time, a high-spatial reconstruction algorithm with a 20-cm field of view, and mediastinal (level, 40 HU; width, 400 HU) and lung (level, −600 HU; width, 1600 HU) window settings. GGO was defined as a misty increase in lung attenuation without obscuring the underlying vascular markings. We defined solid tumor size as the maximum dimension of the solid component measured on lung window settings, excluding GGO.[8] CT scans were reviewed and tumor sizes were determined by radiologists from each institution.

FDG-PET/CT

Patients were instructed to fast for at least 4 hours before intravenous injection of 74 to 370 MBq FDG and were then advised to rest for at least 1 hour before FDG-PET/CT scanning. Blood glucose levels were calculated before the tracer injection to confirm a level of more than 150 mg/dL.[11] Patients with blood glucose levels of 150 mg/dL or more were excluded from the PET/CT imaging. For imaging, Discovery ST (GE Healthcare, Little Chalfont, United Kingdom), Aquiduo (Toshiba Medical Systems Corporation, Tochigi, Japan), or Biograph Sensation 16 (Siemens Healthcare, Erlangen, Germany) integrated 3-dimensional PET/CT scanner was used. Low-dose nonenhanced CT images of 2- to 4-mm section thickness for attenuation correction and localization of lesions identified by PET were obtained from the head to the pelvic floor of each patient according to a standard protocol.

Immediately after CT, PET was performed with the identical axial field of view for 2- to 4-min/table position, depending on the condition of the patient and the scanner performance. An iterative algorithm with CT-derived attenuation correction was used to reconstruct all PET images with a 50-cm field of view. An anthropomorphic body phantom (NEMA NU2-2001, Data Spectrum Corp, Hillsborough, NC) was used to minimize the variations in SUVs among the institutions.[12] A calibration factor was analyzed by dividing the actual SUV by the gauged mean SUV in the phantom background to decrease interinstitutional SUV inconsistencies; the final SUV used in this study is referred to as the revised SUVmax.[13,14] When the SUVmax ratio was expressed as the SUVmax of each institute relative to the SUVmax of the control institute, the adjustment of interinstitutional variations in SUV narrowed the range from 0.89-1.24 to 0.97-1.18. The original SUVmax values were determined by radiologists from each institution.

Follow-up Evaluation

All patients who underwent lung resection were followed up from the day of surgery. Postoperative follow-up procedures, including a physical examination and chest radiograph every 3 months and chest and abdominal CT examinations every 6 months, were performed for the first 2 years. Subsequently, a physical examination and chest radiograph were performed every 6 months, and a chest CT examination was performed every year.

Statistical Analysis

Data are presented as numbers (percent) or the median unless otherwise stated. The χ^2 test for categorical variables was used to compare frequencies, and Fisher's exact test was applied to small samples in all cohorts. McNemar tests were used to analyze the propensity-matched pair patients. Both t tests and Mann-Whitney U tests were used to compare continuous variables in all cohorts. Wilcoxon tests were used to analyze propensity-matched pair patients. Recurrence-free survival (RFS) was defined as the time from the day of surgery until the first event (relapse or death from any cause) or last follow-up. Overall survival (OS) was defined as the time from the day of surgery until death from any cause or the last follow-up. The Kaplan-Meier method was used to analyze the duration of RFS and OS; the Cox proportional hazard model was used to assess differences in RFS and OS. We applied propensity score matching to balance the assignment of the included patients and to correct for the operative procedure (lobectomy or segmentectomy), which confounded survival calculations. The variables were age, gender, solid tumor size, SUVmax, side, and lobe. Because no segmentectomy was performed for a tumor located at a middle lobe, we excluded patients who underwent middle lobectomy from the scoring for a fair comparison. Each variable was multiplied by